## 2025 S.T. Yau High School Science Award (Asia)

## **Research Report**

#### The Team

Registration Number: Chem-049

Name of team member: GE Tanliang

School: The Chinese Foundation Secondary School

Country: Hong Kong, China

Name of supervising teacher: HO Chun Man

Job Title: Deputy School Principal

School: The Chinese Foundation Secondary School

Country: Hong Kong, China

## **Title of Research Report**

Dual Functional Catalyst for Green Hydrogen Production

## **Date**

14 August 2025

#### **Dual Functional Catalyst for Green Hydrogen Production**

#### **GE Tanliang**

#### Abstract

Hydrogen is often proposed as a zero-carbon fuel alternative, but most commercially produced hydrogen comes from fossil fuels, causing environmental harm. To address this, researchers are exploring eco-friendly methods like "green hydrogen" through water electrolysis using renewable electricity. However, water electrolysis faces challenges due to the slow oxygen evolution reaction (OER) and high thermodynamic voltage requirements, as well as the expensive cathodic catalyst for hydrogen evolution reaction (HER). One emerging trend is using urea as an alternative carrier for hydrogen generation. Urea offers advantages like high energy density, non-toxicity, and stability. It can be electrochemically oxidized to convert its chemical energy into electricity, aiding energy conversion and storage. Nonetheless, the complex kinetics of urea electrolysis necessitate a high-performance catalyst for the urea oxidation reaction (UOR).

In this study, a novel approach to fabricate dual functional catalyst with 3D hierarchical nanoarray structures for efficient UOR and HER were proposed. 1D nanoarray structured  $Cu_xNi_{1-x}S$  based catalysts were prepared through alkaline oxidation of Cu foam for developing 1D  $Cu(OH)_2$  nanoarrays, followed by hydrothermal treatment of the as-prepared  $Cu(OH)_2$ @Cu with nickel precursor and thiourea in different conditions.

The resulting Cu<sub>x</sub>Ni<sub>1-x</sub>S based catalysts exhibited exceptional catalytic performance on both UOR and HER. The nano-architecture of the catalyst enables efficient charge transport, electrode stability and catalytic activity toward UOR and HER, allowing the catalyst with lower overpotential (1.417 V for UOR, and -0.271V for HER at 100 mA cm<sup>-2</sup>), smaller Tafel slope (117 mV dec<sup>-1</sup> for UOR, and 204 mV dec<sup>-1</sup> for HER at 100 mA cm<sup>-2</sup>) and higher TOF value (24.4 ms<sup>-1</sup> at 1.50 V for UOR, and 1.625 s<sup>-1</sup> at -0.250 V for HER). The rate of production of hydrogen gas is about 0.365 mmol hr<sup>-1</sup> in urea-assisted hybrid water electrolysis at applied voltage of 1.80 V, with 6.08 mg dm<sup>-3</sup> cm<sup>-2</sup> s<sup>-1</sup> urea degradation rate. The coulombic efficiency of our modal is about 67.3%, with 32.7% loss in ohmic losses and polarization of electrode. Such rare-earth element free Cu<sub>x</sub>Ni<sub>1-x</sub>S@Cu nanoarrays opens the possibility of developing an effective electrocatalyst at a low production cost by simple preparation process for solar-driven urea-assisted hydrogen production via hybrid water electrolysis.

**Keywords**: Dual functional electrocatalyst, copper-nickel-based catalyst, nanoarray structure, hydrogen evolution reaction (HER), urea-oxidation reaction (UOR)

# Acknowledgement

Appreciation goes to the Guangzhou Yahong Testing Technology Company for their technical support on the EDX/elemental mapping analysis, and my schoolmate TAI Cho Fung Woody who will study abroad in September 2025.

## **Commitments on Academic Honesty and Integrity**

#### We hereby declare that we

- 1. are fully committed to the principle of honesty, integrity and fair play throughout the competition.
- 2. actually perform the research work ourselves and thus truly understand the content of the work,
- 3. observe the common standard of academic integrity adopted by most journals and degree theses.
- 4. have declared all the assistance and contribution we have received from any personnel, agency, institution, etc. for the research work.
- 5. undertake to avoid getting in touch with assessment panel members in a way that may lead to direct or indirect conflict of interest.
- 6. undertake to avoid any interaction with assessment panel members that would undermine the neutrality of the panel member and fairness of the assessment process.
- 7. observe the safety regulations of the laboratory(ies) where the we conduct the experiment(s), if applicable.
- 8. observe all rules and regulations of the competition.
- 9. agree that the decision of YHSA(Asia) is final in all matters related to the competition.

We understand and agree that failure to honour the above commitments may lead to disqualification from the competition and/or removal of reward, if applicable; that any unethical deeds, if found, will be disclosed to the school principal of team member(s) and relevant parties if deemed necessary; and that the decision of YHSA(Asia) is final and no appeal will be accepted.

(Signatures of full team below)

Name of team member: GE Tanliang

vanie of team member. GE Tannan

Name of supervising teacher: HO Chun Man

Noted and endorsed by

T.S. Ho

Name of school principal: HO Tik Shun

## **Table of Contents**

Section I	Introduction	6
Section II	Experimental Section	9
	Materials	9
2.2	Preparation of Cu(OH) <sub>2</sub> Nanorod Arrays on Copper Foam	9
	Transformation from Cu(OH) <sub>2</sub> to Cu <sub>x</sub> Ni <sub>1-x</sub> S Nanorod Arrays on Copper Foam	9
2.4	Material Characterizations	11
2.5	Electrochemical Studies	11
Section III	I Results and Discussion	13
3.1	In-situ Growth of 1D 1D Cu(OH) <sub>2</sub> Nanoarray on Cu Foam	13
3.2	Transformation of Cu(OH) <sub>2</sub> @Cu to Cu <sub>x</sub> Ni <sub>1-x</sub> S@Cu via Hydrothermal Treatment	16
3.3	EDX and Elemental Mapping Analysis	18
3.4	Electrochemical Properties – Performance towards HER	20
3.5	Electrochemical Properties – Performance towards UOR	26
3.6	Durability and Stability Studies	29
3.7	Hybrid Water Electrolysis Studies	30
Section V	T Conclusion & Suggestions	33
Appendix		34
Refe	aranca	3.1

#### **Section I** Introduction

Although hydrogen is often suggested as an alternative fuel with zero carbon emissions, the majority of commercially produced hydrogen fuel is produced via steam reforming of hydrocarbons, which are derived from the refining of fossil fuels. This reliance on finite fossil fuel reserves, coupled with their detrimental environmental impact, has spurred researchers to explore eco-friendly methods of hydrogen production. One such method is the production of "green hydrogen" through water electrolysis, which utilizes electricity from renewable sources and takes advantage of the abundant availability of water. However, the efficiency of water electrolysis is hampered by the sluggish oxygen evolution reaction (OER), which necessitates a high thermodynamic voltage of 1.23 V<sup>1</sup>. In electrolyzers, due to ohmic losses and polarization of electrode reactions (especially anodic OER), the real voltage is usually ~1.8 V or more. From the perspective of catalysts, noblemetal-based catalysts are usually used due to their outstanding performance. Therefore, aiming to develop commercial green H<sub>2</sub> production via water electrocatalysis, the most significant issue is to reduce the costs from these two parts: (1) replacing the OER with energy-efficient reactions and (2) using earth-abundant electrocatalysts.

To address the energy requirements of hydrogen generation, there has been a growing trend in utilizing urea as an alternative carrier for hydrogen generation to meet energy demands. This trend is driven by urea's desirable properties such as high energy density, non-toxicity, stability, and nonflammability. Urea is an abundant compound, commonly found as a byproduct in protein metabolism and wastewater contamination. It has shown promise as a hydrogen-rich fuel source, containing approximately 6.7 wt% gravimetric hydrogen content, and higher energy density than compressed or liquid hydrogen which make urea a potential energy carrier (Figure 1.1).

Commound	Donaity / a am-3	Gravimetric H <sub>2</sub>	Volumetric H <sub>2</sub> density /	Energy density
Compound	Density / g cm <sup>-3</sup>	density / % H <sub>2</sub>	$kg H_2 dm^{-3}$	$/ MJ dm^{-3}$
Compressed H <sub>2</sub>	0.039	100	0.039	5.6
Liquid H <sub>2</sub>	0.071	100	0.071	10.1
Aqueous NH <sub>3</sub> (28%)	0.747	2.4	0.13	12.6
Liquid NH <sub>3</sub>	0.747	17.6	0.13	12.6
Urea	1.335	10.07	0.134	16.9

Figure 1.1 Comparison of energy density of different fuels

Notably, there is 2 to 2.5 wt% urea from mammal urine, which means that an additional 0.5 million tons of fuel could be produced annually from human urine alone (240 million tons per year). Electrochemical oxidation of urea has proven to be an effective strategy for both urea conversion and wastewater treatment. By utilizing the urea oxidation reaction (UOR), the chemical energy stored in urea can be converted into electricity. UOR plays a crucial role in various energy conversion and storage technologies due to its significantly lower thermodynamic onset potential (0.37 V) compared to that of OER (1.23 V). With a favorable thermodynamic potential of 0.37 V, UOR seems to be a very promising approach to reduce energy consumption by decreasing the theoretically necessary open circuit voltage, replacing the OER.

At anode  $CO(NH_2)_2(aq) + 6OH^-(aq) \longrightarrow N_2(g) + CO_2(g) + 5H_2O + 6e^-$ 

At cathode  $2H_2O(1) + 2e^- \longrightarrow H_2(g) + 2OH^-(aq)$ 

Overall  $CO(NH_2)_2(aq) + H_2O(1) \longrightarrow N_2(g) + 3H_2(g) + CO_2(g)$ 

However, the actual electrolysis cell voltages for water and urea are still high. The high overpotential of urea electrolysis is due to the fact that anodic UOR is a complex process that involves 6 electrons transfer resulting in sluggish kinetics. The sluggish kinetics of the UOR remains a challenge for the practical implementation of urea electrolysis. Hence, a high-performance catalyst for UOR has been demanded.

Noble metal catalysts like platinum (Pt) and rhodium (Rh) have been traditionally employed to enhance the oxidation process, their high cost and limited long-term performance make them less practical. Recent studies have shown that common transition metals and their oxides, particularly nickel, can achieve similar success at much lower material costs.

Researchers have made significant progress in exploring nickel-based materials for efficient urea oxidation reaction (UOR). For instance, ultrathin and porous nickel hydroxide nanosheets demonstrated a large current density of 298 mA cm<sup>-2</sup> at 1.82 V (vs reversible hydrogen electrode, RHE). Two-dimensional nickel-based metal-organic framework (MOF) nanosheets by coordinating nickel ions and benzenedicarboxylic acid exhibited better UOR performance and lower overpotential compared to Ni(OH)<sub>2</sub> and commercial Pt/C catalysts. Additionally, Ni-MOF with various morphologies such as nanowires, neutrons, and urchins, achieved a current density of 160 mA cm<sup>-2</sup> at approximately 1.8 V (vs RHE). These previous studies have contributed to a comprehensive understanding of the electrocatalytic behavior of nickel-based materials, establishing them as promising candidates for UOR. However, there remains a challenge in addressing the sluggish kinetics of UOR at the anodic area, primarily due to multielectron transfer and multiple gas adsorption/desorption processes. To tackle this issue, researchers consider the coordination of high surface area materials with conductive properties as advantageous for expanding the electrochemically active surface area.

The preparation of heteroatomically nickel based with self-supported three-dimensional (3D) catalysts has emerged as an effective approach to enhance the electrochemical performance of catalysts. In this regard, recent research has focused on exploring Ni-based catalysts for HER and UOR, which has shown promising improvements in catalytic activity. However, the exploration and development of lithium-ion batteries has led to a drastic increase in the demand for key elements such as lithium, nickel, and cobalt, and it is no doubt that the choice of metal needs to swift from Ni-based to another metal with high abundance.

In this study, we aim at developing a novel approach to fabricate 3D hierarchical nanoarray structures for both HER and UOR reaction, and hence to study the feasibility of replacing traditional expensive Pt-based catalyst. Initially, 1D  $Cu(OH)_2$  nanoarrays are directly grown on copper foam, which provided a promising architecture with a large surface area, efficient electron transport, intimate electrolyte access, and structural integrity. Owing to the poor catalytic activity of  $Cu(OH)_2$ , the chemical composition of catalyst,  $Cu(OH)_2$ , is modified as  $Cu_xNi_{I-x}S$  via hydrothermal treatment with  $Ni^{2+}(aq)$  and thiourea solution. This process resulted in the creation of an integrated 3D hierarchical bimetallic (Cu-Ni) sulphide 1D nanoarrays on 3D copper foam with good catalytic performance, structural integrity, stability, and robustness. This integration ensured a

uniform dispersion of the bimetallic sulphide catalyst within the hierarchical structure. The resulting P-doped  $Cu_xNi_{1-x}S_2$  based catalysts exhibited exceptional catalytic performance on both UOR and HER. The nanoarchitecture of the catalyst enables efficient charge transport, electrode stability and catalytic activity toward UOR and HER, allowing the catalyst with lower overpotential(1.417 V for UOR, and -0.271V for HER at 100 mA cm<sup>-2</sup>), smaller Tafel slope (117 mV dec<sup>-1</sup> for UOR, and 204 mV dec<sup>-1</sup> for HER at 100 mA cm<sup>-2</sup>) and higher TOF value (24.4 ms<sup>-1</sup> at 1.50 V for UOR, and 1.625 s<sup>-1</sup> at -0.250 V for HER). The rate of production of hydrogen gas is about 0.365 mmol hr<sup>-1</sup> in urea-assisted hybrid water electrolysis at applied voltage of 1.80 V. The coulombic efficiency of our modal is about 67.3%, with 32.7% loss in ohmic losses and polarization of electrode. Our works open up the possibility of developing an effective electrocatalyst at a low production cost by simple preparation process for solar-driven urea-assisted hydrogen production via hybrid water electrolysis.

#### Section II Experimental Section

#### 2.1 Materials

Chemical reagents including copper foam, sodium hydroxide, potassium peroxydisulphate (K<sub>2</sub>S<sub>2</sub>O<sub>8</sub> Acros) and urea (CO(NH<sub>2</sub>)<sub>2</sub> Acros) were used as received without further purification. Copper foam was rinsed with detergent water, dilute hydrochloric acid and deionized water several times to remove surface impurities.

#### 2.2 Preparation of Cu(OH)<sub>2</sub> Nanorod Arrays on Copper Foam

The copper hydroxide nanostructures were prepared by immersion method. A solution with  $(NH_4)_2S_2O_8$  and NaOH (in mole ratio of 1 : 24) was prepared by dissolving all chemical at 4 °C. A copper foam strip (2 cm  $\times$  4 cm) was immersed in the solution, without stirring, for 1 to 45 minutes [Figure 2.1]. After the immersion, the foam was then rinsed with deionized water to remove excess NaOH or  $(NH_4)_2S_2O_8$ , and dried at 50 °C. Cu foam with 1D Cu(OH)<sub>2</sub> nanoarrays was denoted as Cu(OH)<sub>2</sub>@Cu.



Figure 2.1 (a) Left: Alkaline oxidation of Cu form for preparing 1D Cu(OH)<sub>2</sub> nanoarrays

(b) Right: Cu form under the alkaline oxidation treatment at different durations, from 1 min to 45 minutes

## 2.3 Transformation from Cu(OH)<sub>2</sub> to Cu<sub>x</sub>Ni<sub>1-x</sub>S Nanorod Arrays on Copper Foam

 $1D \ Cu(OH)_2$  nanoarrays were then heated hydrothermally in a mixture of  $Ni^{2+}(aq)$  and thiourea solution in various mole ratios to prepare a series of  $1D \ Cu_xNi_{1-x}S$  nanostructure, which x refers to the proportion of Cu to Ni. Typically, a  $Cu(OH)_2$ @Cu foam  $(1 \ cm \times 2 \ cm)$  was immersed in  $36 \ cm^3$  of solution with different volume ratios of  $2 \ mM \ Ni^{2+}(aq)$  and  $10 \ mM$  thiourea inside the autoclave. The whole mixture was then heated hydrothermally at  $120 - 150 \ ^{\circ}C$  for  $12 \ hours$ . Afterwards, as-prepared samples were thoroughly rinsed with deionized water with the help of sonication, followed by dried at  $70 \ ^{\circ}C$ . [Figure 2.2 and 2.3]



Figure 2.2 (a) Left:  $Cu(OH)_2$ @Cu foams and a solution with different mole ratio of  $Ni^{2+}(aq)$  and thiourea in the autoclave.

(b) Right: Autoclaves were sealed tightly for hydrothermal heating



Figure 2.3 (a) Left: Samples were heated hydrothermally at 120 – 150 °C for 12 hours.

(b) Right: Final Cu<sub>x</sub>Ni<sub>1-x</sub>S@Cu foam

#### 2.4 Material Characterizations

Scanning electron microscopy (SEM) measurements were carried out by using a Hitachi TM4000 plus (operated at 15 kV) to investigate the morphology and surface roughness of samples (Figure 2.2).



Figure 2.2 (a) Left: Mounting the sample for SEM analysis

(b) Middle: Fixing the sample inside the vacuum chamber for degassing

(c) Right: Samples under SEM analysis

#### 2.5 Electrochemical Studies

All the electrochemical measurements were performed with various catalyst utilizing a typical three-electrode system of CHI605E electrochemical workstation (Chenhua Instruments, Shanghai) at room temperature in a 1 M KOH aqueous electrolyte for HER and OER. 2 identical catalyst electrodes and Ag/AgCl were used as a working electrode, counter electrode, and reference electrode, respectively. All potentials were reported vs reversible hydrogen electrode (RHE) based on the equation:

$$E_{RHE} = E_{Ag/AgCl} + 0.0591 \times pH + E_{Ag/AgCl}^{\Theta}$$

where  $E^{\Theta}_{Ag/AgCl} = 0.197$  V at 25 °C, and  $E_{Ag/AgCl}$  is the potential measured vs the Ag/AgCl reference electrode. The current density was normalized to the geometrical area of the electrode, and all polarization curves were corrected for an ohmic drop.

The UOR/OER and HER activities were evaluated by linear sweep voltammetry (LSV) curves at potential values of -0.023 V to +0.800 V (UOR/OER) and -1.000 V to -1.600 V (HER) verse the saturated Ag/AgCl electrode at a scan rate of 10 mV s<sup>-1</sup>. Polarization curves were collected after 95% *iR* correction to compensate for the electrolyte resistance. The potential at current density of 10, 50 and 100 mA cm<sup>-2</sup> were measured for comparison. Pt foil electrodes were used as the reference to compare the activity of UOR and HER by various  $Cu_xNi_{1-x}S@Cu$  samples.

The electrochemical kinetics of the catalyst is evaluated from the Tafel slope, which is based on the linearity equation:  $\eta = a + b \log j$ , where  $\eta$  and j represent overpotential and current density, respectively, and b is the Tafel slope. The steeper the slope, the higher the activation energy required for UOR / HER to occur and slower the reaction rate. The reaction with a small Tafel slope between 30 to 120 mV dec<sup>-1</sup> indicates the rate of reaction is limited by the transfer of electrons to the electrode surface and they are called activation-control reaction. The reaction with an intermediate Tafel slope between 60 to 120 mV dec<sup>-1</sup> shows that the

rate of reaction is limited by the transfer of both electrons and chemical species, e.g. urea, from or to the electrode surface. Chronopotentiometry was performed under a constant current density of 10 mA cm<sup>-2</sup>.

The turnover frequency (TOF) is defined as the specific activity of a catalytic centre for a special reaction under defined reaction conditions by the number of molecular reactions or catalytic cycles occurring at the centre per unit time. It can be calculated by assuming 100% faradaic efficiency with the following equation<sup>17</sup>:

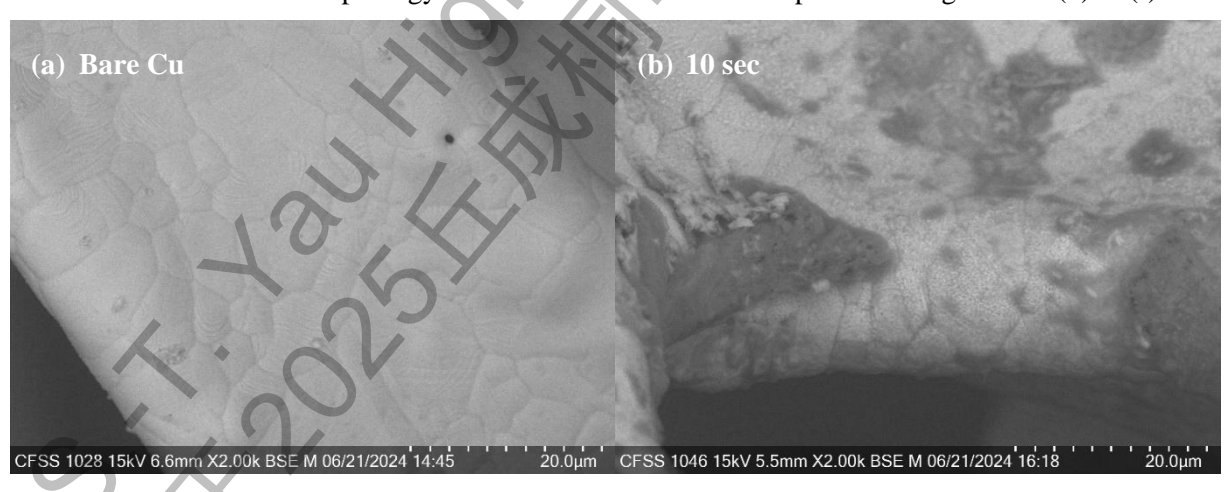
$$TOF = \frac{jS}{\alpha Fm}$$

where j is the current density, S is the area of the electrode;  $\alpha$  represents the electron transfer number in UOR, which is 6, and 2 for HER, F is the Faraday constant (96,485 C mol<sup>-1</sup>); and m is the number of moles of catalyst.

#### **Section III** Results and Discussion

## 3.1 In-situ Growth of 1D 1D Cu(OH)<sub>2</sub> Nanoarray on Cu Foam

The in-situ formation of 1D Cu(OH)<sub>2</sub> nanoarray structure was realized by the chemical oxidation of commercial Cu foam. The morphology of nanostructures at different stages were examined and confirmed by scanning electron microscope (SEM) analysis. Several identical Cu foams were immersed into the mixture of NaOH(aq) or (NH<sub>4</sub>)<sub>2</sub>S<sub>2</sub>O<sub>8</sub>(aq), and they were removed from the solution at different time intervals (10, 20, 40, 60, 120, 300, 600 seconds respectively). All samples were rinsed and dried before the SEM analysis. SEM micrographs were taken at different magnification power (1000x, 1500x and 2000x respectively). Representative SEM micrographs of bare Cu foam and Cu foam with nanostructures, Cu(OH)<sub>2</sub>@Cu, are shown in Figures 3.1 (a) to (h). In Figure 3.1 (a), it can be seen that the surface of pure bare copper is very smooth, and cylindrical Cu(OH)<sub>2</sub> nanostructure has not yet formed. Bare Cu Surface continues to exhibit a plate like morphology. White color in the micrograph indicates that smooth and polished surfaces produce weak contracts with SE imaging. After 10 seconds alkaline oxidation [Figure 3.1 (b)], the surface begins to form a color or gradient difference with darken region found, which indicates that the smooth polished bare Cu surface starts to have chemical erosion by strong alkali, NaOH(aq), giving the rough Cu surface. The surface roughness further increases in the prolonged alkaline treatment. Some small needle-like structures are even found in Figure 3.1 (c). After 40 seconds (Figure 3.1(d)), very tiny needle-shaped Cu(OH)<sub>2</sub> nanostructures are extensively grown on the copper foam on a large scale. The nanoarray structures are vertically and homogenously grown onto the Cu foam skeleton without the assistance of any binder after the chemical oxidation reaction. Similar morphology and nanoarchitecture are also present in Figures 3.1 (d) to (f).



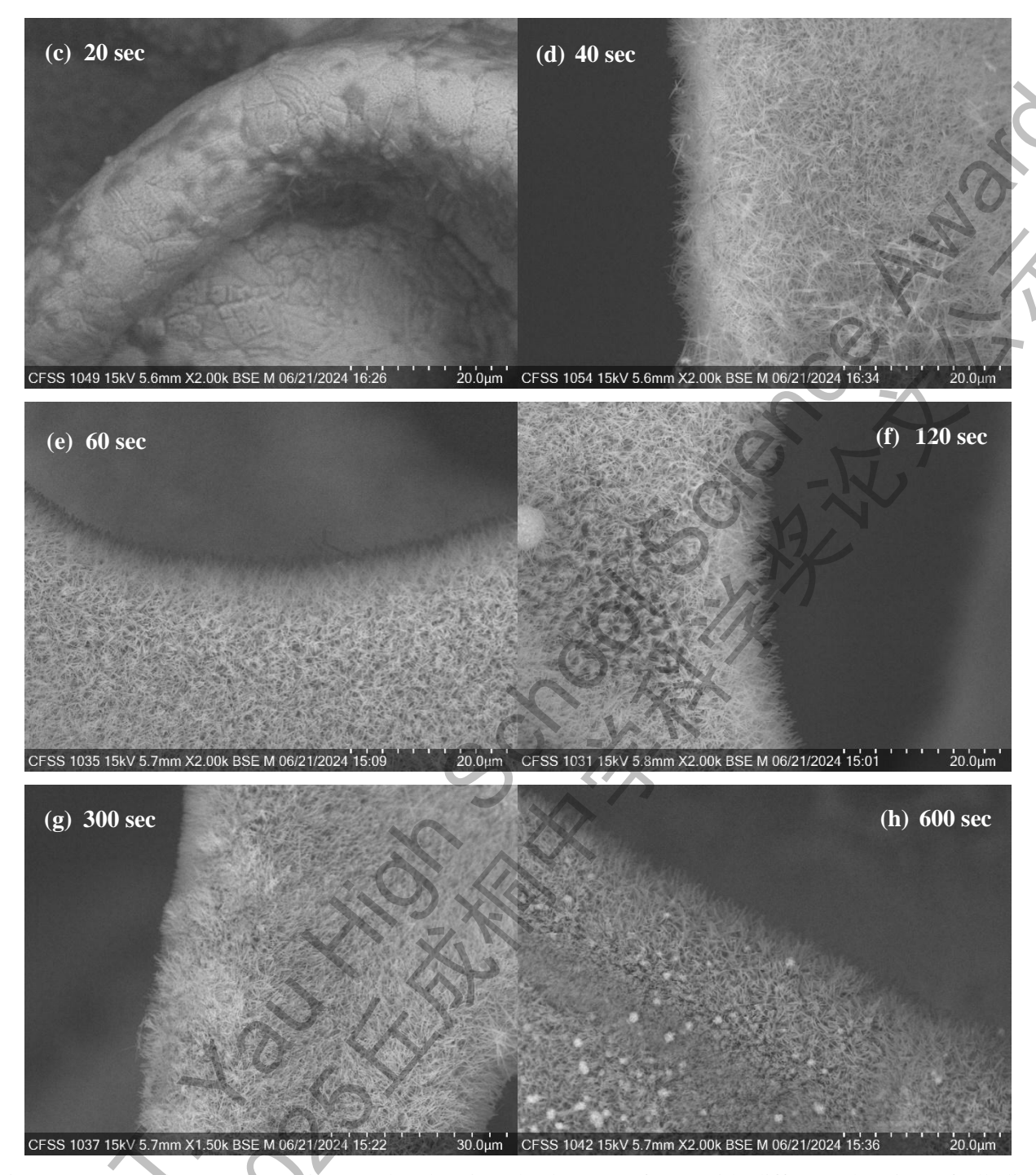


Figure 3.1 (a) to (h) SEM micrographs showing the bare Cu foam with different duration of alkaline oxidative treatment 0, 10, 20, 40, 60, 120, 300, 600 seconds respectively

Figures 3.1 (g) and (h), extensive needle-like protrusions with a densely packed surface are observed, comparing with other micrographs, the volume, surface area, areal density of needle-like nanostructures reached the maximum after soaking in the solution for 600 seconds. At the same time, there were some cubelike crystals on the surface of the sample, which was not the desired result. The spots on the surface of the Cu foam may be caused by the over crystal formation.

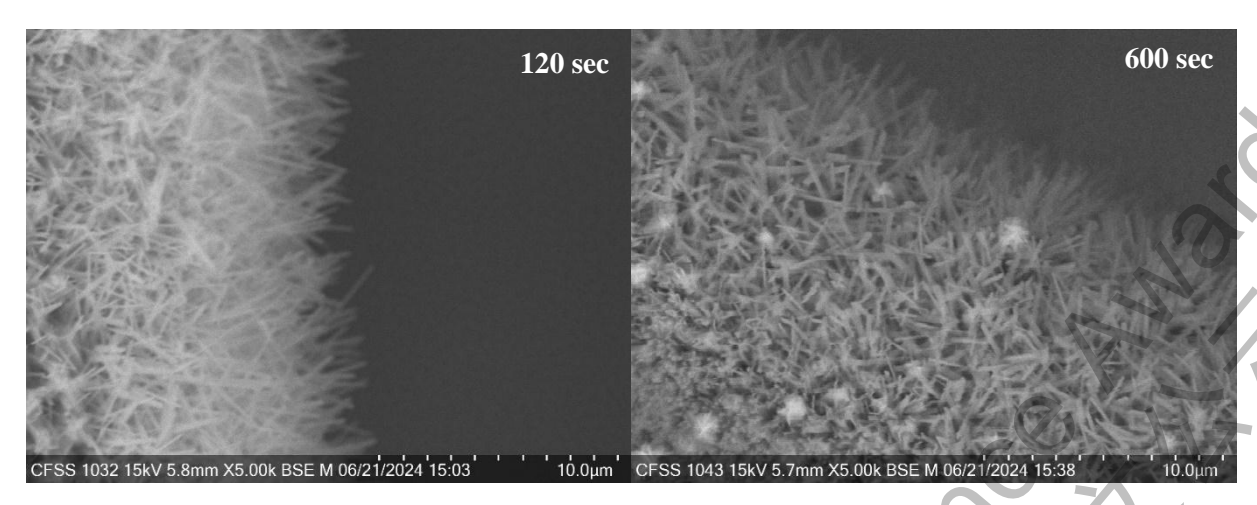


Figure 3.2: Cu(OH)<sub>2</sub> nanostructures in high magnification. Samples under 120 seconds (Left) and 600 seconds (Right) alkaline oxidation.

Figure 3.2 reveals uniform 1D  $\text{Cu}(\text{OH})_2$  nanoarrays developed on the copper foam with relatively uniform width of 100 nm and lengths ranging from 5 to 7  $\mu$ m (based on SEM image estimations), in bottom-to-top directions from its surface. A large aspect ratio is thus achieved in the range of 50 to 70.

The orderly alignment of 1D nanoarray structure on copper foam provides hierarchical structure with both macropores and mesopores, with extensive resistance-free pathway, which facilitate the diffusion of ions or molecules between electrode and diffusion layer of solution film, and large surface area-to-volume ratio for redox reactions. Therefore, as prepared  $Cu(OH)_2@Cu$  foam is used as the basic building block for preparing  $Cu_xNi_{1-x}S$  or others nanoarray structure on Cu foam as an efficient electrochemical catalyst, which can be fabricated by chemical oxidation of Cu by alkaline  $(NH_4)_2S_2O_8$ , followed by hydrothermal treatment [Figure 3.3]

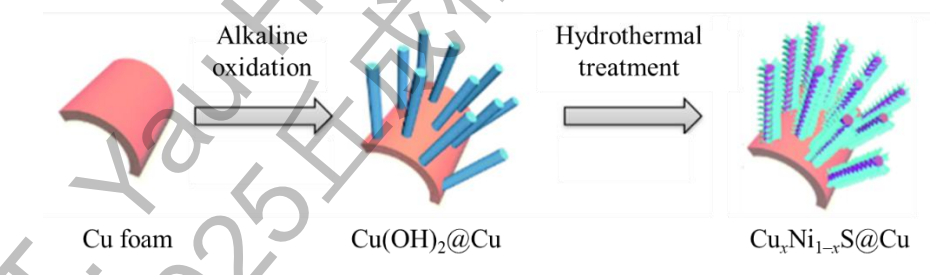


Figure 3.3 Schematic diagram of synthesis of Cu<sub>x</sub>Ni<sub>1-x</sub>S nanoarrays on Cu foam

## 3.2 Transformation of Cu(OH)<sub>2</sub>@Cu to Cu<sub>x</sub>Ni<sub>1-x</sub>S@Cu via Hydrothermal Treatment

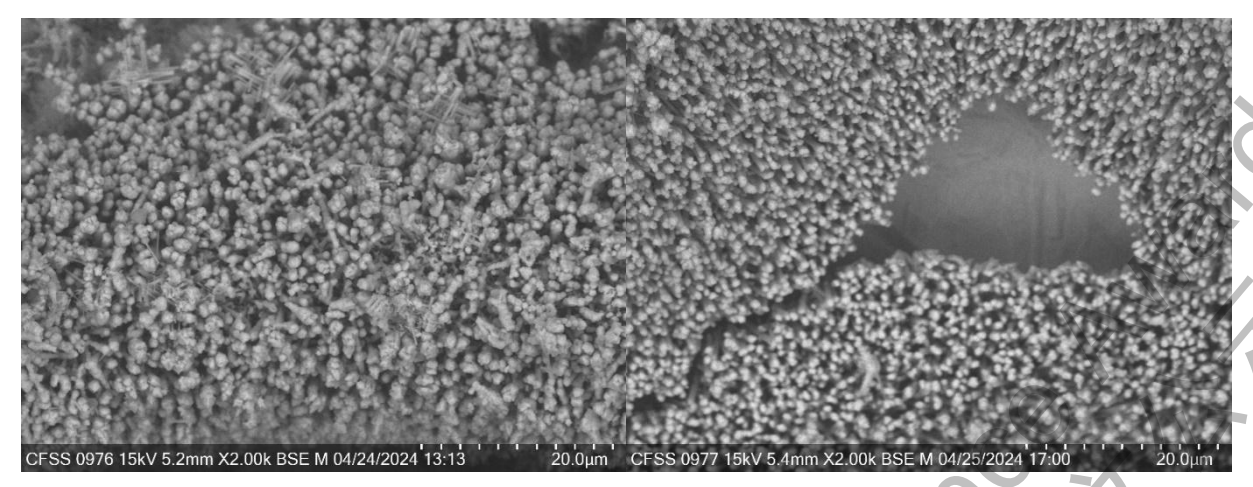
A series of  $Cu_xNi_{1-x}S@Cu$  catalyst was synthesized by hydrothermal treatment by heating a mixture of  $Ni^{2+}(aq)$  and thiourea solution in various mole ratio and  $Cu(OH)_2@Cu$  to prepare a series of  $Cu_xNi_{1-x}S$  nanostructure. Typically, various concentrations of  $Ni^{2+}(aq)$  and thiourea were mixed to give a solution with atomic % (Ni to S) from 20% to 100% (mole ratio from 1:5 to 1:1) for hydrothermal treatment at different conditions from 120 °C to 150 °C for 12 to 15 hr.

Our target is to prepare a  $Cu_xNi_{1-x}S$  nanoarray structure on Cu foam, and one of the primary successful criteria is the preservation of nanoarray structure after the hydrothermal treatment, as well as the quality and uniformness of  $Cu_xNi_{1-x}S$  nanoarray. From SEM results, it is found that the nanoarray structure can only be preserved at low hydrothermal temperature and low concentrations of 1.0 mM  $Ni^{2+}(aq)$ . High temperature and high  $Ni^{2+}(aq)$  concentration (2.0 mM) definitely led to the destruction of the nanoarray structure, as shown in Figure 3.4 (a) and (b). An irregular small lump of crystals is found on the tip of the nanoarray structure. It can be explained by the high concentration of  $Ni^{2+}(aq)$  and hence large amount of nucleation site for crystallization. The nucleation site is particularly originated at the sharp / point region.

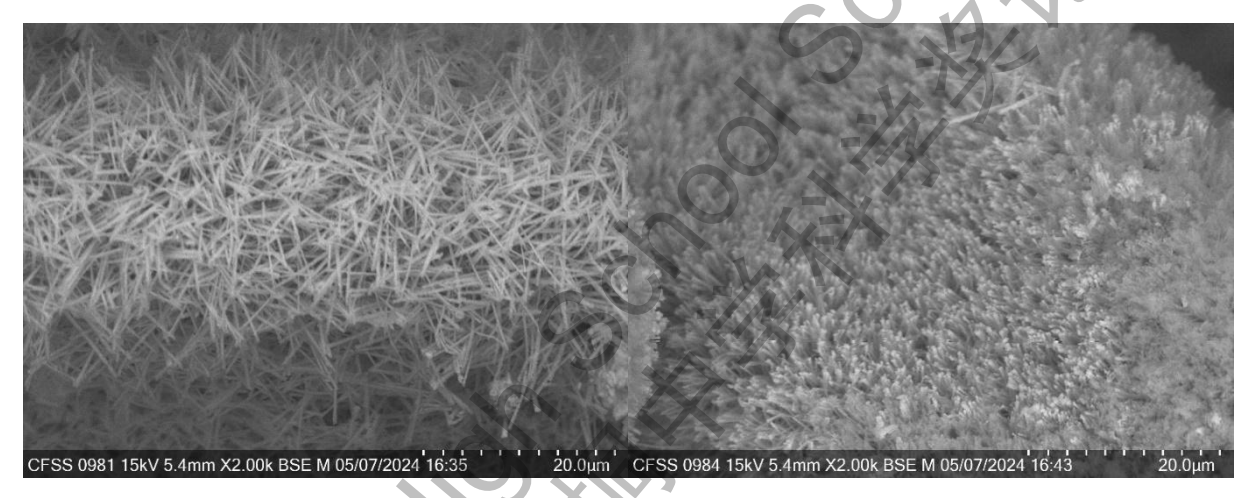


Figures 3.4 (a) and (b):  $Cu_xNi_{1\rightarrow x}S$  nanostructures (prepared by 2 mM  $Ni^{2+}$ (aq) and 150 °C hydrothermal heating) in atomic % (Ni/S) of 50% (left) and 25% (right) respectively

Such unfavorable structures can be avoided by decreasing hydrothermal temperature and  $Ni^{2+}(aq)$  concentration. Unwanted nanostructure cannot be found in Figures 3.4 (c) to (d), with lower-temperature hydrothermal treatment. Yet, the needle-like nanostructures in Figures 3.4 (c) and (d) exhibited a relatively small aspect ratio. The ideal  $Cu_xNi_{1-x}S$  can be successfully prepared from lower  $Ni^{2+}(aq)$  concentration (1.0 mM), as shown in Figures 3.4 (e) and (f).

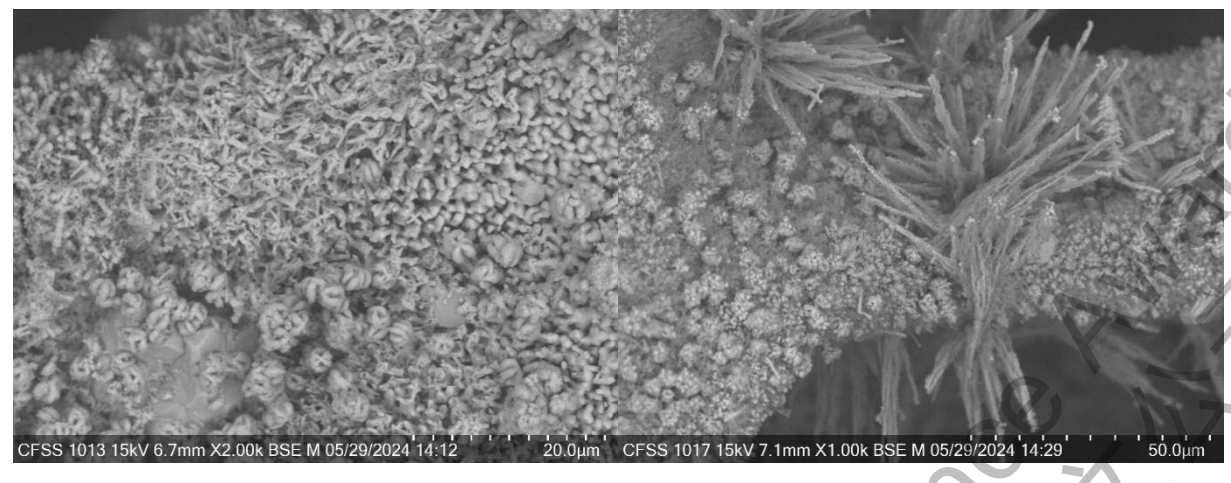


Figures 3.4 (c) and (d): Cu<sub>x</sub>Ni<sub>1-x</sub>S nanostructures (prepared by 2 mM Ni<sup>2+</sup>(aq) and 120 °C hydrothermal heating) in atomic % (Ni/S) of 50% (left) and 25% (right) respectively

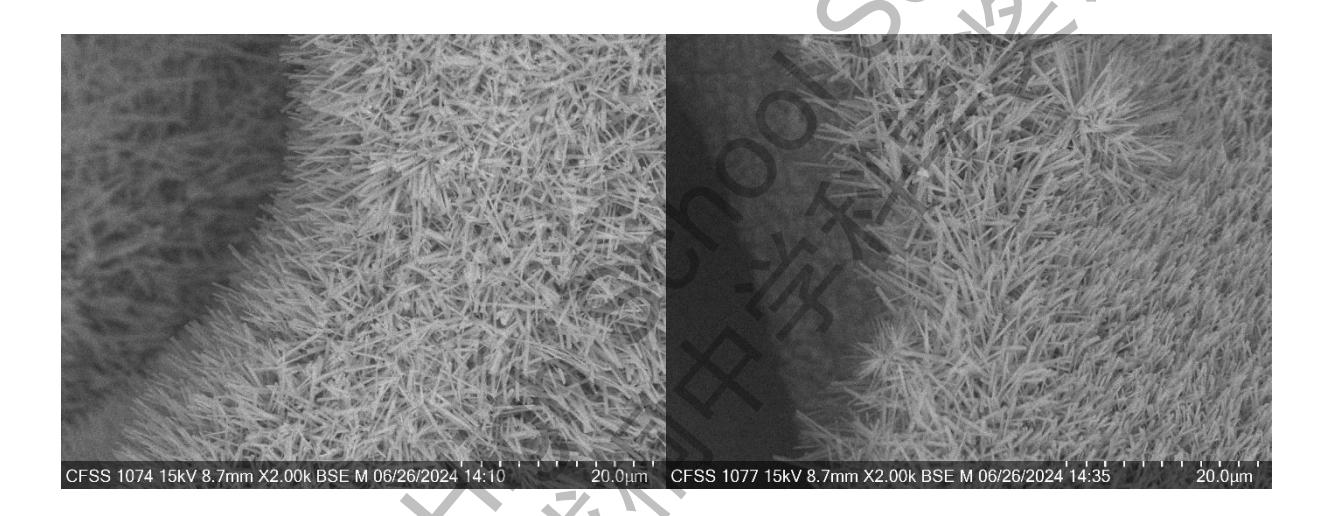


Figures 3.4 (e) and (f):  $Cu_xNi_{1-x}S$  nanostructures (prepared by 1 mM  $Ni^{2+}$ (aq) and 120 °C hydrothermal heating) in atomic % (Ni/S) of 50% (left) and 25% (right) respectively

Besides the hydrothermal temperature and  $Ni^{2+}$ (aq) concentration, samples with various atomic % (Ni/S), ranging from 20 to 100 are fabricated. Generally, samples with lower atomic % of Ni show a well-structured nanoarray pattern, with little or even no defect. Figures 3.4 (g) and (h) display the  $Cu_xNi_{1-x}S$  crystal in high atomic % (Ni/S) of 70 to 100. Well-structured nanoarray patten is completely deformed and large heterostructure crystals can be easily observed. On the other hand, samples in lower level of Ni atomic % (generally less than 45%) exhibit a high degree of structural preservation.



Figures 3.4 (g) and (h):  $Cu_xNi_{1-x}S$  nanostructures (prepared by 1 mM  $Ni^{2+}$ (aq) and 120 °C hydrothermal heating) in atomic % (Ni/S) of 75% (left) and 50% (right) respectively



Figures 3.4 (i) and (j):  $Cu_xNi_{1-x}S$  nanostructures (prepared by 1 mM  $Ni^{2+}(aq)$  and 120 °C hydrothermal heating) in atomic % (Ni/S) of 25% (left) and 20% (right) respectively

## 3.3 EDX and Elemental Mapping Analysis

The composition and elemental distributions of  $Cu_xNi_{1-x}S$  were examined by SEM/EDX mapping. Figures 3.5 (a) are the image of elemental mapping of  $Cu_xNi_{1-x}S$ . The atomic ratio of Cu:Ni:S is calculated as 11.5: 2.3: 1.0. The high atomic ratio of Cu in the EDX analysis can be rationalized from the proposed mechanism mentioned in Figure 3.3. As the copper foam is used as the substrate and the signal for Cu should be dominant. Moreover, the prepared  $Cu(OH)_2@Cu$  foam is used as the basic building block and foundation structure for transforming to  $Cu_xNi_{1-x}S$  composition. The  $Cu_xNi_{1-x}S$  transformation only takes part on the surface of  $Cu(OH)_2$  nanoarray, while the interior part remains chemically unchanged.

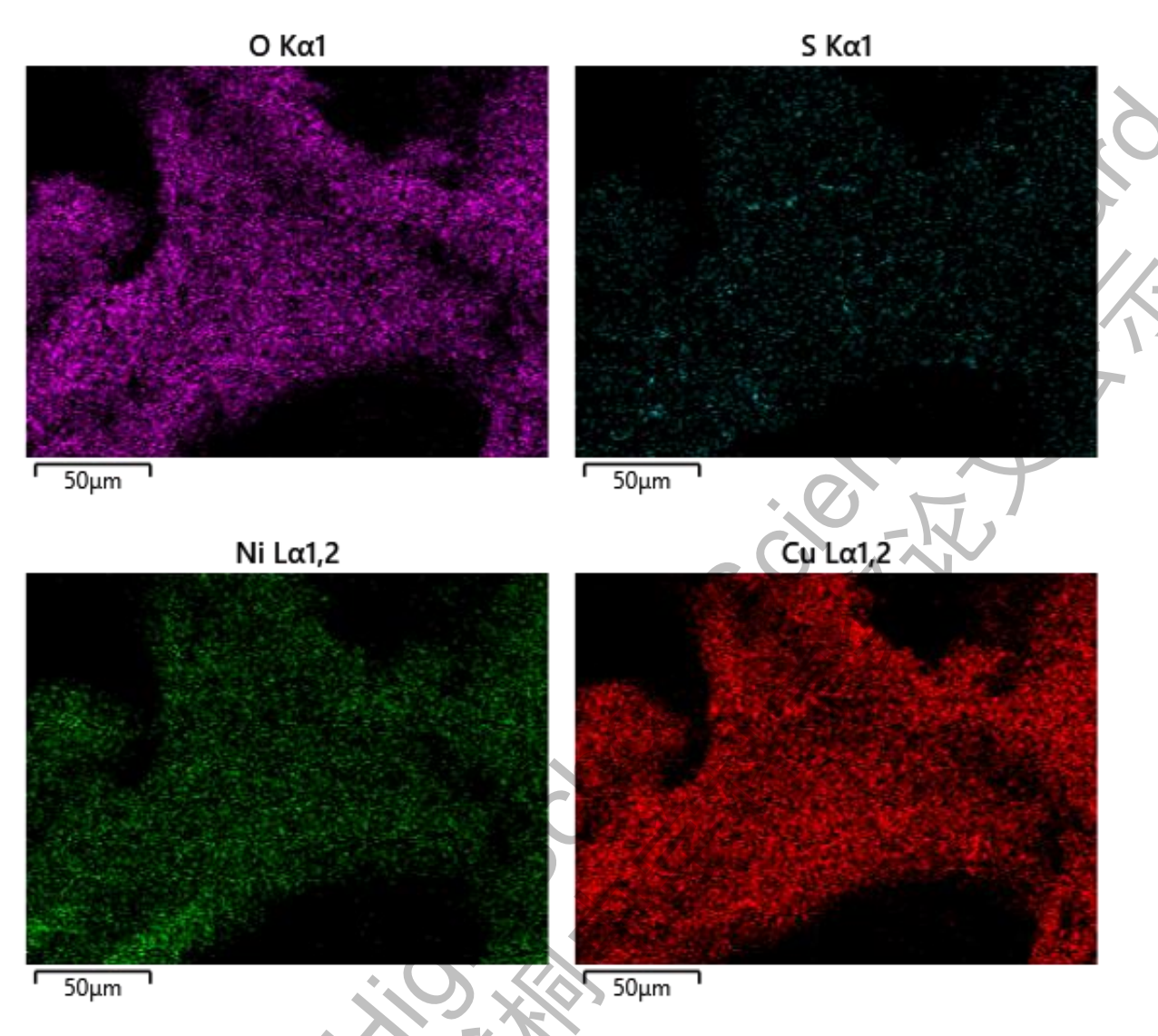


Figure 3.5 (a) to (d) The element mapping of  $Cu_xNi_{1-x}S$  samples.

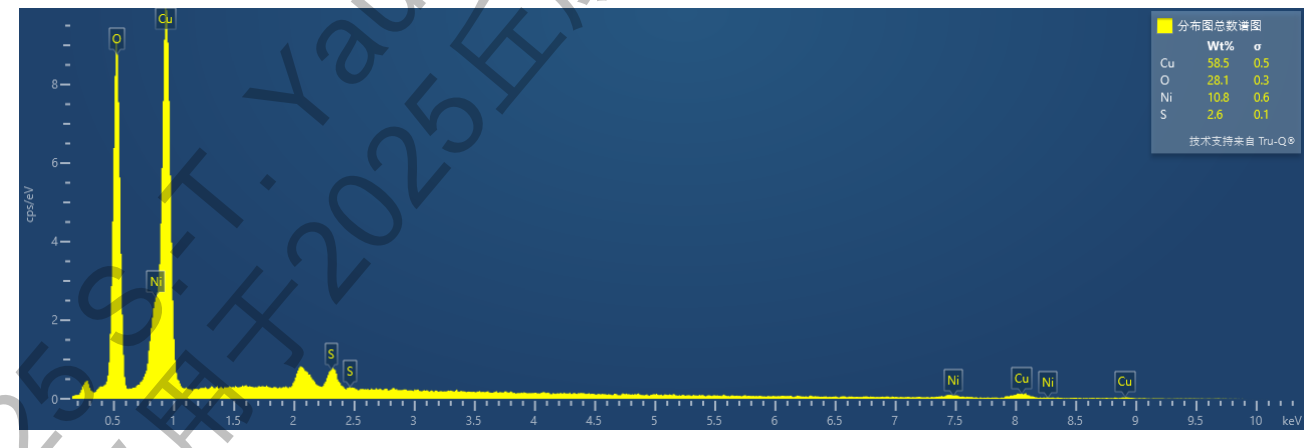


Figure 3.5 (e) The EDX spectrum of  $Cu_xNi_{1-x}S$  samples

## 3.4 Electrochemical Properties – Performance towards HER

The as-prepared electrodes were directly used as the working electrode for electrocatalytic performance evaluation. The electrochemical performance of catalysts toward the UOR and HER (electrolyte: 1 KOH with 0.33M urea or 1 M KOH) at a scan rate of 10 mV s<sup>-1</sup> was evaluated through a conventional three-electrode configuration. The iR-compensated linear sweep voltammetry (LSV) curves of the series of catalysts for both UOR and HER were plotted. A urea oxidation reaction (UOR) and hydrogen evolution reaction (HER) in an alkaline environment can be expressed as follows:

Anode:  $CO(NH_2)_2(aq) + 6OH^-(aq) \longrightarrow N_2(g) + 5H_2O(l) + CO_2(g) + 6e^-$ 

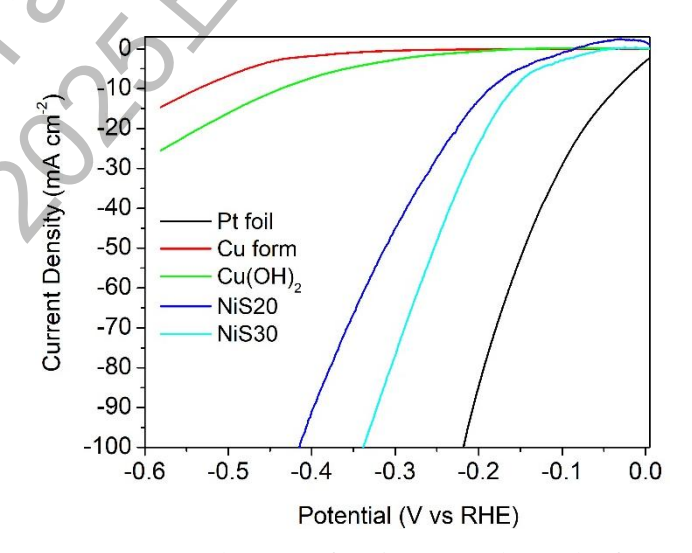
Cathode:  $2H_2O(1) + 2e^- \longrightarrow H_2(g) + 2OH^-(aq)$ 

Overall:  $CO(NH_2)_2(aq) + H_2O(1) \longrightarrow N_2(g) + 3H_2(g) + CO_2(g)$ 

The nanoarray structure of all samples were re-confirmed by SEM before LSV test, and they are denoted as NiSx such as NiS20, NiS30, where x refers to the atomic % of Ni over S, and they are prepared by 1 mM Ni<sup>2+</sup>(aq) and 120 °C hydrothermal heating. HER performances of various samples are compared with various reference such as precious metal catalyst Pt, and copper base (Figure 3.6 (a)). From the results, it is clearly shown that neither Cu foam nor Cu(OH)<sub>2</sub> nanostructure is an efficient material as the electrocatalyst for HER and both of them low activity on HER (–536 mV and –436 mV for current density at 10 mA cm<sup>-2</sup>). Nevertheless, the performance shows a significant improvement when the sample is incorporated with nickel and sulphur, which displays better performance with lower applied potential to reach the same current density, 242 mV and 355 mV decrease in NiS20 and Ni30 respectively.

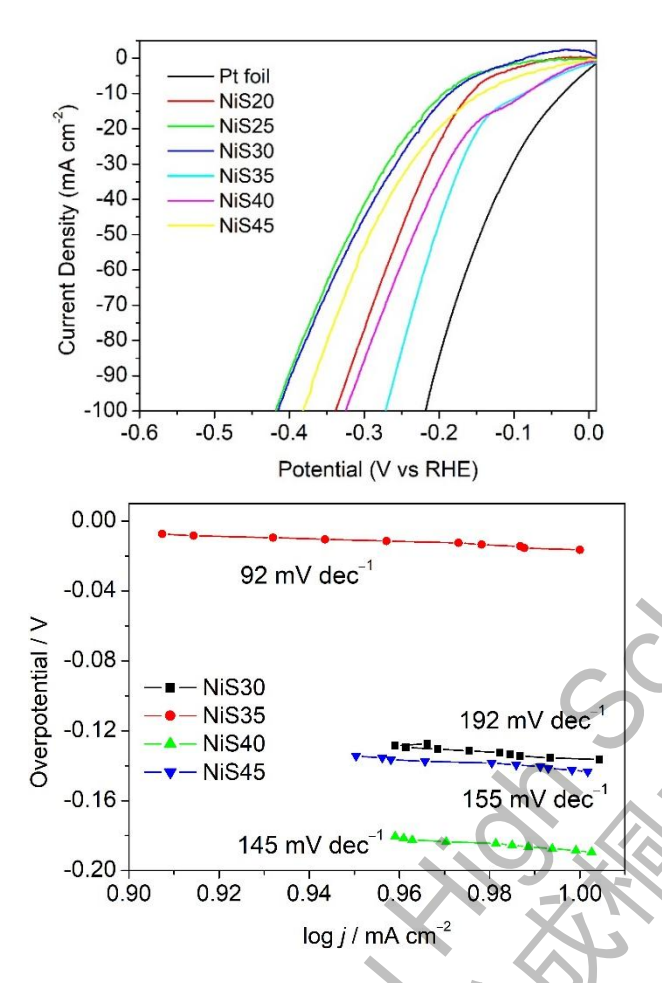
	Potential at the corresponding current density $j / V$ (V vs RHE)					
Current density	Pt	Cu	Cu(OH) <sub>2</sub>	NiS20	NiS30	
10 mA cm <sup>-2</sup>	-0.035	-0.536	-0.436	-0.186	-0.081	

Table 3.2 Summary of respective potential at current density of 10 cm<sup>-2</sup> of various samples and reference.



Figures 3.6 (a) LSV curves towards HER of various samples and references.

To further investigate the relationship between catalytic activity and nickel, sulphur content, various samples with different atomic ratio of Ni and S are incorporated into  $Cu(OH)_2$  array through hydrothermal treatment. The performances of samples with different atomic % of Ni/S are summarized in Figure 3.6 (b) – (d) and their performances are compared with Pt electrode as reference and Table 3.3.



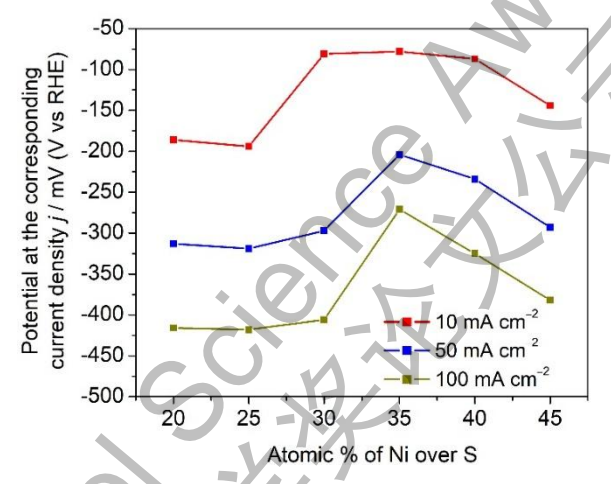


Figure 3.6: (b) LSV curves towards HER of various  $Cu_xNi_{1-x}S$  samples (top right); (c) Potential at corresponding current density j (10, 50 and 100 mA cm<sup>-2</sup> respectively) in the function of atomic % of Ni (top left); (d) Tafel plots of NiSx (x = 30 to 45) in 1.0 M KOH(aq) (left).

	Potential (towards HER) at the corresponding current density $j / V$ (V vs RHE)							
Current density	Pt	NiS20	NiS25	NiS30	NiS35	NiS40	NiS45	
10 mA cm <sup>-2</sup>	-0.034	-0.186	-0.194	-0.081	-0.078	-0.087	-0.144	
50 mA cm <sup>-2</sup>	-0.146	-0.313	-0.319	-0.297	-0.204	-0.234	-0.293	
100 mA cm <sup>-2</sup>	-0.219	-0.416	-0.418	-0.406	-0.271	-0.325	-0.382	

SO &X	Tafel slope / mV dec <sup>-1</sup>						
Current density	Pt	NiS20	NiS25	NiS30	NiS35	NiS40	NiS45
10 mA cm <sup>-2</sup>	95	171	232	197	92	145	155
50 mA cm <sup>-2</sup>	209	271	288	272	183	288	322
100 mA cm <sup>-2</sup>	246	376	392	377	204	384	500

Table 3.3 Summary of respective potential and Tafel slope at the corresponding current density (10, 50 and  $100 \text{ cm}^{-2}$ ) from the  $\text{Cu}_x \text{Ni}_{1-x} \text{S}$  with different atomic % (Ni/S) (20% to 45%) and reference (Pt foil).

As shown in Figure 3.6 (b), the cathodic potential of all  $Cu_xNi_{1-x}S$  electrocatalysts for the HER decreases considerably when the potential drops to -0.20 V, which indicates the reduction current increased under the action of electrocatalyst, thus demonstrating that HER taking place at the electrode. It was found that the activity of HER over the catalyst depends on the Ni content. Cathodic potential for HER increases (becomes less negative) from 20% Ni (-186 mV) to 35% Ni (-78 mV), and then declines afterwards. Similar pattern can also be observed at current density of 50 and 100 mA cm<sup>-2</sup> respectively. Smaller overpotential (less negative) means less energy is required to initiate the HER at considerable rate. The change in cathodic potential is even more significant at higher current density, indicating that the sample is more efficient at high current density. Concluded from above results, the most promising electrocatalyst should be prepared from  $Ni^{2+}$ (aq) and thiourea in mol ratio of 7 to 20, while electrochemical catalyst NiS35 demonstrates the best performance on HER (Figure 3.6 (e) & (f)).

Tafel plots in Figure 3.6 (c) are provided to unveil the reaction kinetic of the catalyst towards HER. The NiS35 has the most outstanding performance with the smaller Tafel slope in various current density (92, 183 and 204 mV dec<sup>-1</sup> at current density of 10, 50 and 100 mA cm<sup>-2</sup> respectively) compared to that of reference commercial Pt electrode (95, 209 and 246 mV dec<sup>-1</sup> at current density of 10, 50 and 100 mA cm<sup>-2</sup> respectively), as shown in Table 3.3 Most importantly, the value 95 mV dec<sup>-1</sup> is significantly smaller than that required for the HER process (120 mV dec<sup>-1</sup>). The decrease in Tafel slope in NiS35 confirms that the reaction kinetics can be enhanced upon adjusting Ni/S atomic ratio in the catalyst. The abovementioned results show that the rationally designed hierarchical CuNi-sulphide catalyst on 1D Cu(OH)<sub>2</sub> nanoarrays is a highly active catalyst and it has a favorable charge-transfer kinetics towards HER process. The NiS35 exhibits comparable and even superior activities to most of the recent report HER electrocatalyst (Table 3.4).

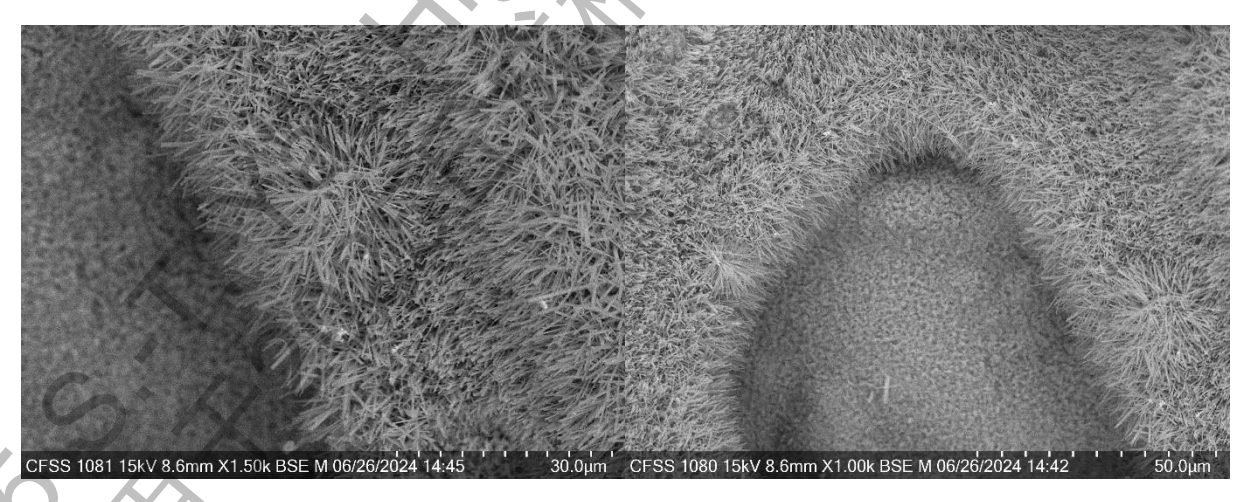


Figure 3.6 (e) & (f) SEM images of NiS35 sample.

Cotolout	Potential at 10 mA cm <sup>-2</sup>	Tafel slo	ppe	Reference	
Catalyst	(mV vs RHE)	(mV dec	<sup>-1</sup> )	Reference	
		10 mA cm <sup>-2</sup>	92	. (	
NiS35	-92	50 mA cm <sup>-2</sup>	183	This work	
		100 mA cm <sup>-2</sup>	204	70	
		10 mA cm <sup>-2</sup>	95	This work	
Pt	-95	50 mA cm <sup>-2</sup>	209	(reference)	
		100 mA cm <sup>-2</sup>	246	(reference)	
NiMo	-154	10 mA cm <sup>-2</sup>	152	ChemElectroChem	
1 1111/10	15 1	To his tem	132	<b>2021</b> , 8, 195	
Ru-MoS <sub>2</sub> /CC	-41	10 mA cm <sup>-2</sup>	114	Appl. Catal. B: Environ	
			6	<b>2021</b> , 249, 91	
NiRu-MOF/NF	-51	10 mA cm <sup>-2</sup>	90	ACS Appl. Mater.	
H-Ni/NiO/C	-87	C	91.7	Interfaces <b>2020</b> , 12, 34728	
NH-Ni/NiO/C	-117	.0	98.7	N. C.	
		10 mA cm <sup>-2</sup>	4 X = / \	Nano Convergence	
H-Ni/C	-167	~ C) ->	106.5	<b>2023</b> , 10:6	
H-NiO/C	-246	5	124.2		
Ni/NiO/NCW-1	-105.3	10 mA cm <sup>-2</sup>	55.2	J. Alloys Compd.	
112/11/10/11/01/1	100.0		33.2	<b>2021</b> , 853, 157338	
Ni/NiO-CNTs	-98	10 mA cm <sup>-2</sup>	79	Appl. Surf. Sci.	
NI/NIO-CN IS	-98	TO HIA CIII	19	<b>2019</b> , 491, 294	
NiO/C	700	10 4 -2	77.0	Journal of Hydrogen	
composite	-565	10 mA cm <sup>-2</sup>	77.8	Energy <b>2019</b> 44, 16144	
NiO	200	5 m A am-2	<i>(</i> 0	J. Power Sources	
NIO	-209	5 mA cm <sup>-2</sup>	60	<b>2015</b> , 300, 336	
NiO/Ni @C C	000	10 mA cm <sup>-2</sup>		Catal. Sci. Technol.	
NiO/Ni@C-O	-89	10 mA cm -	-	<b>2021</b> , 11, 2480	
Ni/NiO	-120	10 mA cm <sup>-2</sup>	114	Angew. Chem.	
1101110	-120	10 m/3 cm	114	<b>2016</b> , 128, 703	

Table 3.4 A detailed HER performance comparison of representative HER catalysts in alkaline media published in the literature

To better compare the catalytic activities of the samples, the turnover frequency (TOF) of various samples and total number of hydrogen turnovers are calculated based on the current density at potential from -0.10 V to -0.40 V, and results are presented as Figure 3.6 (g) and Table 3.5 and 3.6.

The total number of hydrogen turnovers was obtained by the following equation.

$$\begin{split} &\text{no. of H}_2 = \Big(j\frac{\text{mA}}{\text{cm}^2}\Big) \bigg(\frac{1\text{ C s}^{-1}}{1000\text{ mA}}\bigg) \bigg(\frac{1\text{ mol e}^-}{96485.3\text{ C}}\bigg) \bigg(\frac{1\text{ mol H}_2}{2\text{ mol e}^-}\bigg) \bigg(\frac{6.02\times10^{23}\text{ H}_2}{1\text{ mol H}_2}\bigg) \\ &\text{no. of H}_2 = 3.121\times10^{15} \bigg(\frac{\text{H}_2\text{ s}^{-1}}{\text{cm}^2}\bigg) per\bigg(\frac{\text{mA}}{\text{cm}^2}\bigg) \end{split}$$

Importantly, although it makes more sense to consider the actual number of  $Cu_xNi_{1-x}S$  species for a more comprehensive analysis, accurately singling out these  $Cu_xNi_{1-x}S$  species from all the other inactive species, such as those present in Cu substrate presents a formidable challenge. Consequently, TOF is determined by considering all the  $Ni^{2+}$  used in the synthesis as active sites, recognizing that this approach unavoidably leads to an underestimation of the TOF value. The effect of atomic % of Ni of the sample does not show a remarkable change on TOF at lower potential as TOF exhibits in the range from  $0.276 \text{ s}^{-1}$  to  $0.482 \text{ s}^{-1}$ . The improvement becomes more obvious at higher potential that NiS5 demonstrates the highest TOF of  $7.12 \text{ s}^{-1}$  at -0.40 among others, and the results from NiS35 are consistent to other tests mentioned before. Although the TOF cannot be comparable to others shown in Table 3.7 in recent literature. Their catalysts always rely on rare earth metal either Pt or Ru. Our catalysts take advantages in terms of both synthesis easiness and cost of HER, which are fundamental aspects to consider for practical hybrid water electrolysis.

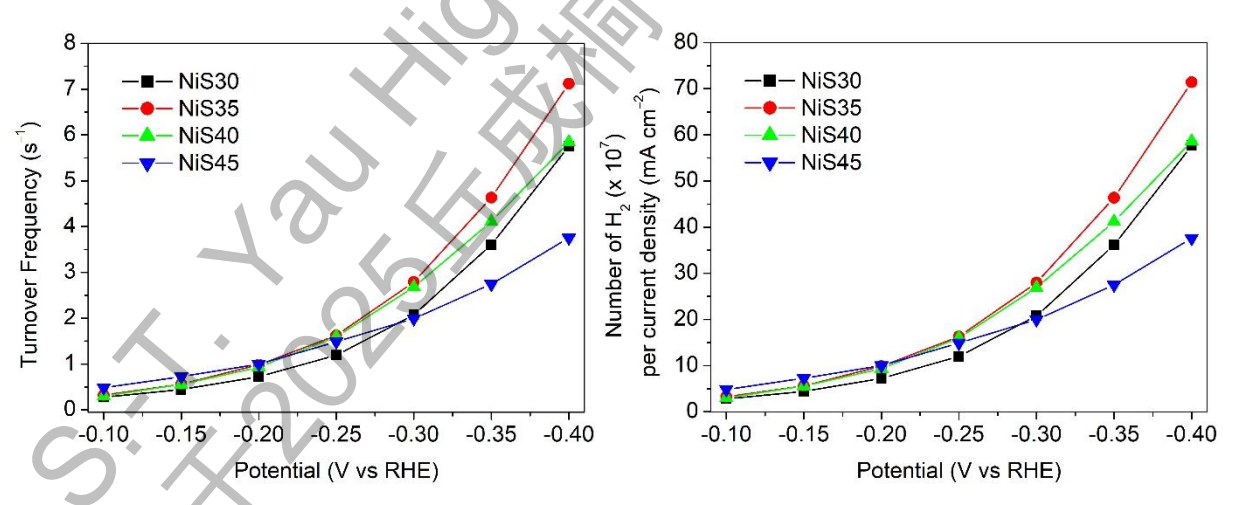


Figure 3.6 (g) TOF plots at various potential of various samples (left); and number of  $H_2$  gas per current density (right)

	Turnover Frequency (towards HER), s <sup>-1</sup>						
Potential, V vs RHE	NiS30	NiS35	NiS40	NiS45			
-0.10	0.276	0.324	0.301	0.482			
-0.15	0.442	0.562	0.555	0.726			
-0.20	0.724	0.985	0.933	0.998			
-0.25	1.193	1.625	1.596	1.487			
-0.30	2.077	2.793	2.682	1.993			
-0.35	3.603	4.633	4.107	2.744			
-0.40	5.754	7.120	5.843	3.755			

Table 3.5 Turnover Frequency (TOF) of various samples at different potential

	Total number of hydrogen turnovers × 10 <sup>7</sup> (s <sup>-1</sup> cm <sup>-2</sup> per mA cm <sup>-2</sup> )						
Potential, V vs RHE	NiS30	NiS35	NiS40	NiS45			
-0.10	2.77	3.25	3.01	4.83			
-0.15	4.43	5.63	5.56	7.27			
-0.20	7.26	9.87	9.35	10.0			
-0.25	12.0	16.3	16.0	14.9			
-0.30	20.8	28.0	26.9	20			
-0.35	36.1	46.4	41.2	27.5			
-0.40	57.7	71,4	58.6	37.6			

Table 3.6 The total number of hydrogen turnovers

	A ZA	
Catalyst	TOF at 100 mV, s <sup>-1</sup>	Reference
NiS35	0.324	This work
Ru@Cu-TiO <sub>2</sub> /Cu	3.85	J. Am. Chem. Soc. 2023, 145, 21419
Ru-Cu-2	0.309	Nano Energy <b>2022</b> , 92, 106763
Ru/D-NiFe LDH	1.27	Nat. Commun. <b>2021</b> , 12, 4587
Pt/Ni <sub>3</sub> S <sub>2</sub> /NF	1.41	ACS Appl. Mater. Interfaces, <b>2020</b> , 12, 39163
RuNi-NSs@PANI	0.0498	J. Catal. <b>2019</b> , 375, 249
Te@Ru-0.6/C	0.82	Chem. Commun. <b>2019</b> , 55, 1490
SrRuO <sub>4</sub>	0.90	Nat. Commun. <b>2019</b> , 10, 149
Ni@Ni₂P-Ru	1.1	J. Am. Chem. Soc. 2018, 140, 2731
Ru@NG	0.776	J. Mater. Chem. A 2018, 6, 13859
Pt-Co-Co/TiM	1.23	Nanoscale <b>2018</b> , 10, 12302

Table 3.7 Comparison between the TOF of various catalysts in 1M KOH / NaOH reported in recent literature.

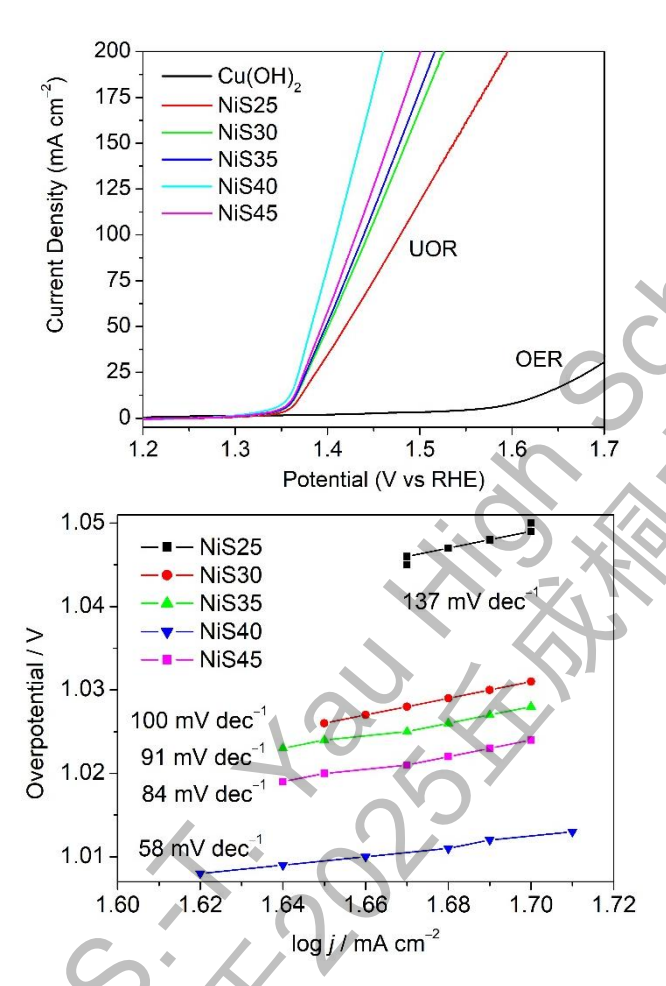
## 3.5 Electrochemical Properties – Performance towards UOR

NiS20 to NiS45 were directly used as the working electrode for electrocatalytic performance evaluation. The electrochemical performance toward the UOR (electrolyte: 1 KOH with 0.33M urea) and OER (electrolyte: 1 M KOH) at a scan rate of 10 mV s<sup>-1</sup> was evaluated through a conventional three-electrode configuration. The iR-compensated linear sweep voltammetry (LSV) curves of the series of catalysts for both OER and UOR were plotted [Figure 3.7]. A urea oxidation reaction in an alkaline environment can be expressed as follows:

Anode:  $CO(NH_2)_2(aq) + 6OH^-(aq) \longrightarrow N_2(g) + 5H_2O(l) + CO_2(g) + 6e^-$ 

Cathode:  $2H_2O(1) + 2e^- \longrightarrow H_2(g) + 2OH^-(aq)$ 

Overall  $CO(NH_2)_2(aq) + H_2O(1) \longrightarrow N_2(g) + 3H_2(g) + CO_2(g)$ 



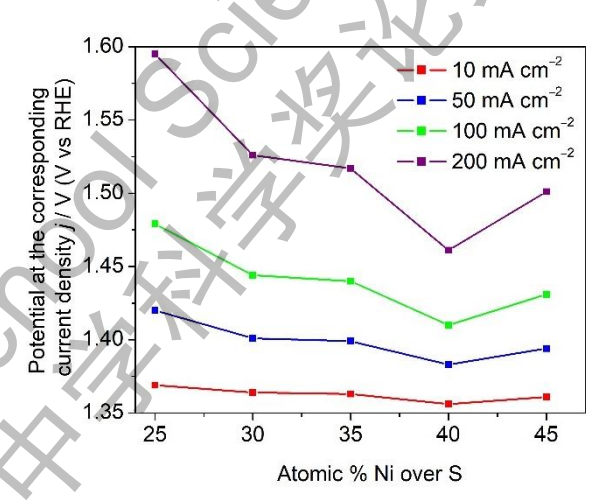


Figure 3.7: (a) LSV curves towards UOR of various  $Cu_xNi_{1-x}S$  samples (top right); (b) Potential at corresponding current density j (10, 50 and 100 mA cm<sup>-2</sup> respectively) in the function of atomic % of Ni (top left); (c) Tafel plots of NiSx (x = 30 to 45) in 1.0 M KOH + 0.33 urea at 50 mA cm<sup>-2</sup> (left).

As shown in Figure 3.7 (a) to (c), the anodic potential of all  $Cu_xNi_{1-x}S$  electrocatalysts for UOR decreases considerably to ~1.4 V to attain a current density of 10 mA cm<sup>-2</sup>, compared to 1.62 V for the OER, which indicates the oxidation current increased considerably in the presence of urea, thus indicating that  $H_2$  production by urea electrolysis was more energy efficient than water electrolysis. Moreover, all catalysts exhibit OER and UOR activities in alkaline media with a drastic increase of the current at ~1.36 V vs RHE in the presence of 0.33 M urea. Results display that the activity of UOR over the catalyst also depends on the Ni/S atomic ratio. The anodic potential for UOR at current density of 200 mA cm<sup>-2</sup> decreases from 25% Ni

(1.48 V) to 40% (1.41 V), and then increases afterwards. Effect of Ni content is even more obvious at high potential in achieved current density from 300 mA cm<sup>-2</sup> to 716 mA cm<sup>-2</sup> at 1.70 V (139% increment). Concluded from above results, the most promising electrocatalyst should be prepared from Ni<sup>2+</sup>(aq) and thiourea in mol ratio of 7 to 20, while electrochemical catalyst NiS40 demonstrates the best performance on UOR. Results in the potential at the corresponding current density of all target samples have been tabulated in Table 37 and 3.8.

	Potential (towa	Potential (towards UOR) at the corresponding current density $j / V$ (V vs RHE)						
Current density	NiS25	NiS30	NiS35	NiS40	NiS45			
10 mA cm <sup>-2</sup>	1.369	1.364	1.363	1.356	1.361			
50 mA cm <sup>-2</sup>	1.420	1.401	1.399	1.383	1.394			
100 mA cm <sup>-2</sup>	1.479	1.444	1.440	1.410	1.431			
200 mA cm <sup>-2</sup>	1.595	1.526	1.517	1.461	1.501			

	Tafel slope / mV dec <sup>-1</sup>					
Current density	NiS25	NiS30	NiS35	NiS40	NiS45	
10 mA cm <sup>-2</sup>	32.3	30.5	31	41.6	33.1	
50 mA cm <sup>-2</sup>	137	100	91.3	57.7	84.4	
100 mA cm <sup>-2</sup>	258	186	184	117	163	
200 mA cm <sup>-2</sup>	518	408	347	223	308	

Table 3.8 Summary of respective potential and Tafel slope at the corresponding current density (10, 50, 100 and 200 mA cm $^{-2}$ ) towards UOR from the Cu<sub>x</sub>Ni<sub>1-x</sub>S with different atomic % (Ni/S) (25% to 45%)

Tafel plots and Tafel slopes summarized in Figure 3.7 (c) and Table 3.8 are provided to unveil the reaction kinetic of the catalyst towards UOR. The NiS40 has the most outstanding performance with the smaller Tafel slope in various current densities (42, 58, 117 and 223 mV dec<sup>-1</sup> at current density of 10, 50, 100 and 200 mA cm<sup>-2</sup> respectively) compared to that of reference commercial RuO<sub>2</sub> catalyst (70 mVdec<sup>-1</sup> at 10 mA cm<sup>-2</sup>). Most importantly, the value 42 mV dec<sup>-1</sup> is about an order of magnitude smaller than that required for the OER process (151 mV dec<sup>-1</sup>). The decrease in Tafel slope in NiS40 confirms that the reaction kinetics can be enhanced upon Ni and S incorporation. The abovementioned results show that the rationally designed hierarchical Cu<sub>x</sub>Ni<sub>1-x</sub>S on 1D Cu(OH)<sub>2</sub> nanoarrays is a highly active catalyst and it has a favorable charge-transfer kinetics towards UOR process.

To quantify the intrinsic activities of the electrocatalysts toward UOR, the turnover frequency of various samples is calculated based on the current density at potential of 1.4 to 1.7 V, and results are presented as Figure 3.8 and Table 3.9. Remarkably, NiS40 demonstrates a high TOF of 24.4 s<sup>-1</sup> at 1.5 V, which is comparable to the reference commercial  $RuO_2$  (25.3 s<sup>-1</sup>).

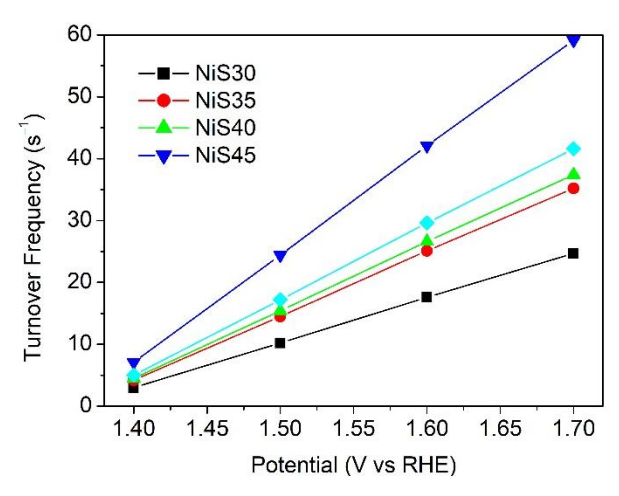


Figure 3.8 TOF plots at various potential of various samples

		Turnover Frequency (towards UOR), ms <sup>-1</sup>						
Potential, V vs RHE	NiS25	NiS30	NiS35	NiS40	NiS45			
1.40	3.0	4.2	4.5	7.1	5.0			
1.50	10.2	14.5	15.4	24.4	17.2			
1.60	17.6	25.1	26.6	42.1	29.6			
1.70	24.7	35.2	37.4	59.1	41.6			

Table 3.9 TOF, towards UOR, of various samples at different potential

## 3.6 Durability and Stability Studies

In addition to the splendid HER activity, a chronoamperometric (V – t) measurement at 100 mA cm<sup>-2</sup> for 40 hours is conducted to evaluate the durability and stability of the NiS35 electrode toward HER. The potential of NiS35 increased by 13 mV after 40 hours stability test. At the same time, a little variation was discerned in LSV curves of NiS35 before and after stability test, further confirming its excellent catalytic activity and high stability (Figure 3.9). From SEM analysis, the morphology and shape of those nanoarrays are well preserved after 40 hours measurement, without serious structural deformation or aggregation, shown in Figure 3.10.

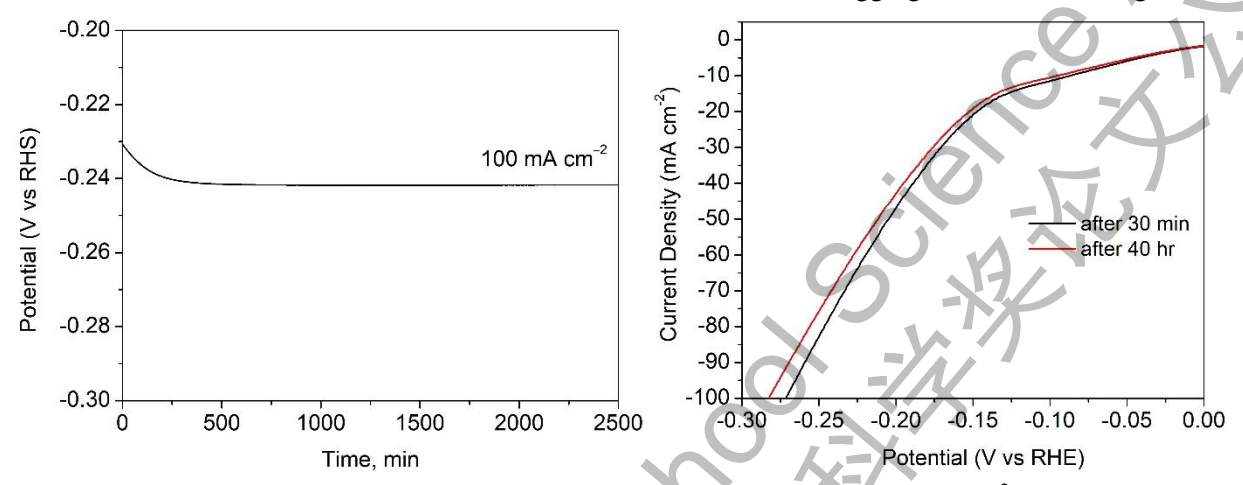


Figure 3.9 Right: Chronoamperometric measurement of NiS35 at 100 mA cm<sup>-2</sup> for 40 h.

Left: LSV curves of NiS35 after 30 min and 40 h chronoamperometric measurement

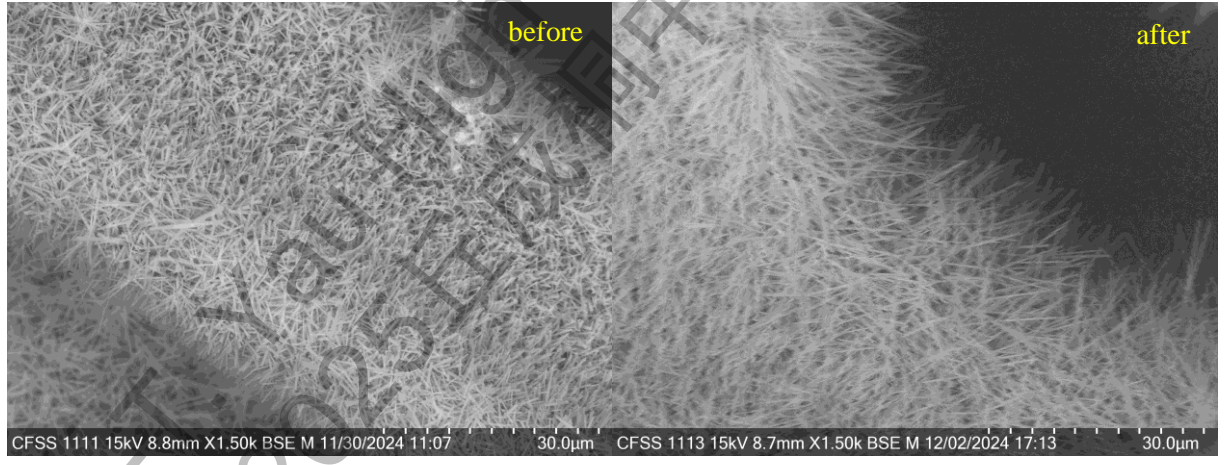


Figure 3.10 SEM images of NiS35 before (left) and after (right) 40 h chronoamperometric measurement

### 3.7 Hybrid Water Electrolysis Studies

UOR is an alternative reaction to replace OER in water electrolysis for producing hydrogen more efficient in view of its lower thermodynamic potential. Additionally, UOR offers the advantage of utilizing urea-rich wastewater as feedstock, and thereby providing a potential solution for urea-rich wastewater purification. The efficiency of hydrogen production was studied by using Hofmann Voltammeter Set-up. As mentioned above, UOR plays a crucial role in various energy conversion and storage technologies due to its significantly lower thermodynamic onset potential (0.37 V) compared to that of OER (1.23 V). With a favorable thermodynamic potential of 0.37 V, UOR seems to be a very promising approach to reduce energy consumption by decreasing the theoretically necessary open circuit voltage, replacing the OER. Therefore, hybrid water electrolysis by incorporating UOR and HER reaction is more energetically favorable ( $E_{appl} = +0.37 \text{ V}$ ) than the conventional method ( $E_{appl} = +1.23 \text{ V}$ )

$$\begin{array}{lll} \text{At anode} & & CO(NH_2)_2(aq) + 6OH^-(aq) & \longrightarrow & N_2(g) + CO_2(g) + 5H_2O + 6e^- & E^\theta_{anode} = 0.37 \text{ V} \\ \text{At cathode} & & 2H_2O(1) + 2e^- & \longrightarrow & H_2(g) + 2OH^-(aq) & E^\theta_{cathode} = 0.00 \text{ V} \\ \text{Overall} & & CO(NH_2)_2(aq) + H_2O(1) & \longrightarrow & N_2(g) + 3H_2(g) + CO_2(g) & E^\theta_{cell} = +0.37 \text{ V} \\ \end{array}$$

Typically, our sample NiS40 and NiS35 are used as anode (for UOR) and cathode (for HER) respectively and they are mounted in rubber stoppers for hydrogen production. A solution with 1.0 M KOH and 0.333 M urea solution is used as the electrolyte for hybrid water electrolysis. The volume of hydrogen gas collected is measured from the column of Hofmann Voltammeter. The coulombic efficiency of the hybrid water electrolysis and faradaic efficiency of HER are evaluated from the following equations.

In view of the reaction at the cathode, the coulombic output can be estimated from the volume of hydrogen gas collected over a fixed time interval using the following equation:

Number of mole of 
$$H_2$$
 gas formed  $(n_{H_2(g)}) = \frac{PV_{H_2(g)}}{RT}$ ,

where P = 101325 N m<sup>-2</sup>;  $V_{H_2(g)} = \text{volume of } H_2(g)$  collected in m<sup>3</sup>; R = 8.314 J mol<sup>-1</sup> K<sup>-1</sup>, T = air temperature at Kelvin Scale and hence the number of coulomb of charge output  $= n_{H_2(g)} \times 2 \times F$ , where F is Faraday constants 96485 C mol<sup>-1</sup>. The coulombic input can be calculated from the area under the graph obtained from the chronoamperometric measurement. Hence, the coulombic efficiency is defined by the following equation:

$$\begin{aligned} & \text{Coulombic efficiency} = \frac{n_{H_2(g)} \times 2 \times F}{i \times t} \\ & \text{Faradaic efficiency} = \frac{n_{H_2(g)}}{\frac{Q}{2 \times F}} \end{aligned}$$

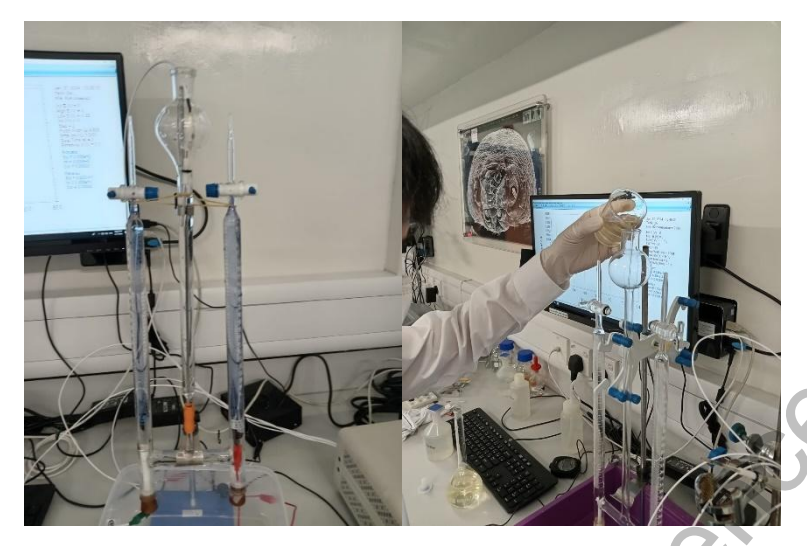


Figure 3.11 (a) Hofmann Voltammeter Set-up for hybrid water electrolysis of water (left).

1 M KOH or a mixture of 1 M KOH and 0.333 M urea are used as electrolyte (right).



Figure 3.11 (b) NiS35 as the cathodic catalyst for HER at cathode. (left)

Volume of hydrogen gas produced is measured from the column of Hofmann Voltammeter (right)

In view of the full-scan LSV curve in Figure 3.12, the significant downshift of the anodic current of OER to UOR with the significant drop in the onset potential, while the cathodic current of Hydrogen Evolution Reaction (HER). Traditionally, the efficiency of water electrolysis is hampered by the sluggish OER, which necessitates a high thermodynamic voltage of 1.23 V. In the practical case, due ohmic losses and polarization of electrode reactions (especially anodic OER), the real onset potential occurred in Figure 3.12 is up to 1.70 V or even higher for larger output current density such as 100 mA cm<sup>-2</sup> at 2.1 V. In order to study the efficiency of urea-assisted hydrogen production via hybrid water electrolysis, the applied voltage should be assigned to less than 2.0 V to ensure OER is energetically unfavorable to happen in this condition. Hence, the applied voltage in hybrid water electrolysis is adjusted to the minimum voltage required for continuous hydrogen gas liberation at cathode, which is determined by LSV measurement. For the measurable amount of hydrogen gas production, the current density on both anodic current (UOR) and cathodic current (HER) should be set at 100 mA cm<sup>-2</sup>, ranging from -0.271 V to +1.410 V verse RHE, with the potential window of 1.681 and therefore

1/-

the applied voltage is 1.80 V using NiS35 as cathode and NiS40 as anode in 0.333 M urea-1 M KOH electrolyte. The result is reconfirmed with no hydrogen gas liberation at cathode in 1 M KOH electrolyte, under 1.80 V applied voltage. The results of volume of hydrogen gas liberated under conventional water electrolysis and urea-assisted hybrid water electrolysis are presented in Figure 3.13.

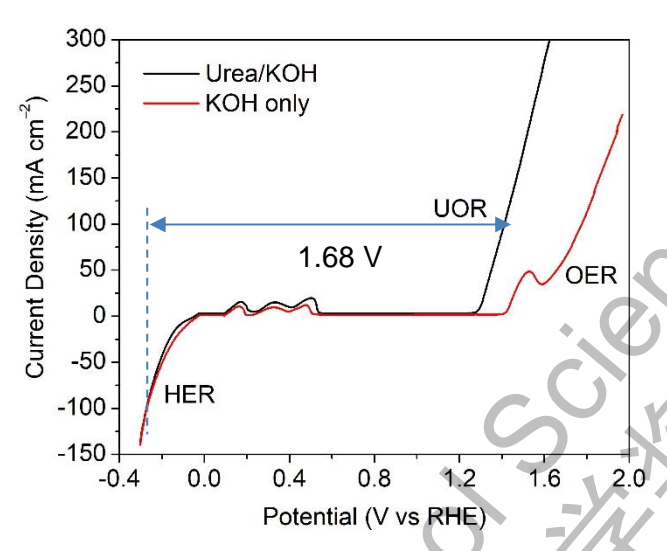


Figure 3.12 Full scan LSV curve for both HER, UOR and OER

As expected, the rate of production of hydrogen gas is about 0.608 mmol cm<sup>-2</sup> hr<sup>-1</sup> and almost 0.0 mmol cm<sup>-2</sup> hr<sup>-1</sup> in urea-assisted hybrid water electrolysis and conventional water electrolysis at applied voltage of 1.80 V. The coulombic efficiency of our model is about 67.3%, with 32.7% loss in ohmic losses and polarization of electrode. It demonstrates the feasibility of developing commercial green  $H_2$  production via urea-assisted hybrid water electrolysis.

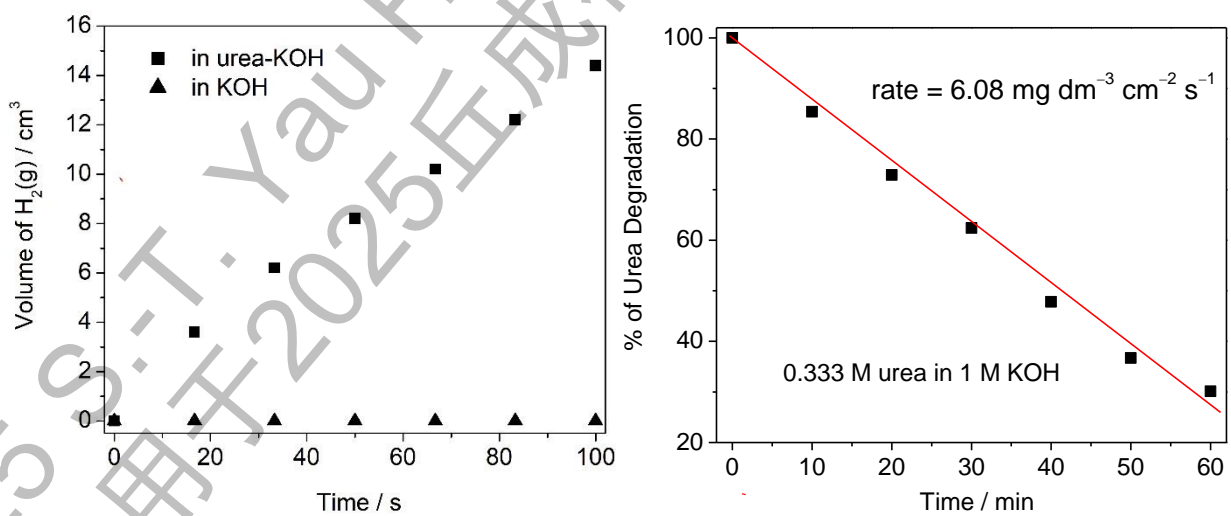


Figure 3.13 Hydrogen gas production via urea-assisted hybrid water electrolysis and conventional water electrolysis

	Rate	Coulombic efficiency	Faradaic efficiency
Urea-assisted H <sub>2</sub> production	$0.608 \; \mathrm{mmol} \; \mathrm{cm}^{-2}  \mathrm{hr}^{-1}$	67.3%	50.0%

#### Section VI Conclusion & Suggestions

In this project, our designed  $Cu_xNi_{1-x}S@Cu$  nanoarrays electrode exhibits promising HER activity. The morphology, materials and structure characterization and the electrochemical properties have been extensively investigated. During this research, several challenging problems needed to be addressed. These include synthesizing the stable  $Cu(OH)_2$  nanoarrays structure on Cu foam, optimizing hydrothermal temperature,  $Ni^{2+}(aq)$  concentration and Ni to S mole ratio and various electrochemical studies.

The nanoarrays structure of  $Cu(OH)_2@Cu$  can be simply prepared by alkaline oxidation treatment of Cu foam. Yet, the transformation of 1D  $Cu(OH)_2@Cu$  to 1D  $Cu_xNi_{1-x}S@Cu$  without serious structural deterioration can only be achieved in the optimum conditions.

The hierarchical structure, morphology and surface roughness have been extensively examined by SEM analysis and their nanoarrays structures are well preserved without deformation after the hydrothermal treatment. The aggregation of crystal can be found at high hydrothermal temperature and high Ni<sup>2+</sup>(aq) concentration, and it definitely causes the different degree of structural deformation.

The dural functional properties of as-prepared catalyst towards HER and UOR are evaluated by various techniques including linear sweep voltammetry, cyclic voltammetry and chronoamperometric measurement. From their polarization curves, all our catalysts exhibit HER and UOR activities in alkaline media, while the NiS35 and NiS40 catalysts display the most superior performance than other nickel-sulphur combinations, with the lowest potential required to achieve considerable current density (only 1.417 V for UOR, and -0.271 for HER at 100 mA cm<sup>-2</sup>) with the smaller Tafel slope and higher TOF, compared to that of reference commercial UOR RuO<sub>2</sub> catalyst.

From our chronoamperometric (V-t) measurement, NiS40 coupled with NiS35 as both anode and cathode exhibits high durability and stability toward continuous urea electrolysis for 40 hours. The potential for HER is just increased by 13 mV after 40 hours stability test, with a little variation in LSV curves of NiS35 catalyst before and after the stability test, further confirming its excellent catalytic activity and high stability

In conclusion, the hierarchical dual functional  $Cu_xNi_{1-x}S@Cu$  nanoarrays as electrocatalyst has been developed with promising electrochemical performance. The nano-architecture of the catalyst enables efficient charge transport, electrode stability and catalytic activity toward UOR and HER, allowing the catalyst with lower overpotential (1.417 V for UOR, and -0.271V for HER at 100 mA cm<sup>-2</sup>), smaller Tafel slope (117 mV dec<sup>-1</sup> for UOR, and 204 mV dec<sup>-1</sup> for HER at 100 mA cm<sup>-2</sup>) and higher TOF value (24.4 ms<sup>-1</sup> at 1.50 V for UOR, and 1.625 s<sup>-1</sup> at -0.250 V for HER), which are more superior than the commercial RuO<sub>2</sub> catalyst. The rate of production of hydrogen gas is about 0.365 mmol hr<sup>-1</sup> in urea-assisted hybrid water electrolysis at applied voltage of 1.80 V. The coulombic efficiency of our modal is about 67.3%, with 32.7% loss in ohmic losses and polarization of electrode. Such rare-earth element free  $Cu_xNi_{1-x}S@Cu$  nanoarrays opens the possibility of developing the effective electrocatalyst in low production cost by simple preparation process for solar-driven urea-assisted hydrogen production via hybrid water electrolysis.

#### **Appendix**

## Reference

- TAI, C. F. W., Ge, T. Research Report for Regeneron International Science and Engineering Fair 2025.
- 2. Xu, W., Zhang, H., Li, G., Wu, Z. Scientific Reports 2014, 4, 5863.
- 3. Lan, R., Tao, S., Irvine, J. T. S. Energy Environ. Sci. 2010, 3, 438-441.
- 4. Zhang, J.-Y.; He, T.; Wang, M.; Qi, R.; Yan, Y.; Dong, Z.; Liu, H.; Wang, H.; Xia, B. Y. *Nano Energy* 2019, 60, 894–902.
- 5. Rollinson, A. N.; Jones, J.; Dupont, V.; Twigg, M. V. Energy Environ. Sci. 2011, 4, 1216 1224.
- 6. Chen, S.; Duan, J.; Vasileff, A.; Qiao, S. Z. Angew. Chem., Int. Ed. 2016, 55, 3804–3808.
- 7. M. Gong, Y. Li, H. Wang, Y. Liang, J.Z. Wu, J. Zhou, J. Wang, T. Regier, F. Wei, H. Dai, *J. Am. Chem. Soc.* 2013, 135, 8452 8455.
- 8. Ge J., Liu, Z., Guan, M., Kuang, J., Xiao, Y., Yang, Y., Tsang, C. H., Lu, X., Yang, C. *J Colloid Interface Sci.* 2022, 620, 442 453.
- 9. Ge J., Lin, L., Wang, S. Q., Wang, Y., Ma, X., An, Q., Zhao, L. J. Mater. Chem. A. 2023, 11, 15100 15121.
- 10. King, R. L., Botte, G. G. J. Power Sources 2011, 196, 9579 9584.
- Lu, S., Hummel, M., Gu, Z., Wang, Y., Wang, K., Pathak, R., Zhou, Y., Jia, H., Qi, X., Zhao, X., Xu, B.
   B., Liu, X. ACS Sustainable Chem. Eng. 2021, 9, 1703 1713.
- 12. Yang, W.; Yang, X.; Li, B.; Lin, J.; Gao, H.; Hou, C.; Luo, X. J. Mater. Chem. A 2019, 7, 26364 26370.
- 13. Zhu, D.; Guo, C.; Liu, J.; Wang, L.; Du, Y.; Qiao, S.-Z. Chem. Commun. 2017, 53, 10906 10909.
- 14. Yuan, M.; Wang, R.; Sun, Z.; Lin, L.; Yang, H.; Li, H.; Nan, C.; Sun, G.; Ma, S. *Inorg. Chem.* 2019, 58, 11449 11457.
- 15. Mao, L, Hao, X., Zhang, Y., Wong, S. Y., He, J., Wang, S., Liu, X., Huang, X., Wang, J., Li, Xu. *ACS Appl. Nano Mater.* 2023, 11, 9857 9864.
- Lee, Y. W., Kim, B. S., Hong, J., Lee, J., Pak, S., Jang, S. P., Jang, H. S., Whang, D., Cha, S. N., Sohn,
   J. I., Kim, J. M. J. Mater. Chem. A, 2016, 4, 10084 10090.
- 17. Sun, H., Liu, J., Chen, G., Kim, H., Kim, S., Hu, Z., Chen, J.-M., Haw, S.-C., Ciucci, F., Jung, W. *Small Methods* 2022, 6, 2101017.
- 18. Sun, H., Li, L., Chen, H-C., Duan, D., Humayun, M., Qiu, Y., Zhang, X., Ao, X., Wu, Y., Pang, Y., Huo, K., Wang, C., Xiong, Y. *Sci Bull*, 2022, 67, 1763 1775
- 19. Zhang, Q., Wang, J., Xu, D., Wang, Z., Li, X., Zhang, K. J. Mater. Chem. A, 2014, 2, 3865 3874.
- 20. Zemtsova, V. M., Oshchepkov, A. G., Savinova, E. R. ACS Catal. 2023, 20, 13466 13473.
- 21. Anuratha, K. S., Rinawati, M., Wu, T. H., Yeh, M. H., Lin, J Y. Nanomaterials, 2022, 12, 2970.
- 22. Sun, H., Liu, J., Kim, H., Song, S., Fei, L., Hu, Z., Lin, H. J., Chen, C. T., Ciucci, F., Jung, W. *Advanced Science*, 2022, 34, 2204800.
- 23. Wu, Y., Liu, X., Han, D. Nat Commun 2018, 9, 1425.

- 24. Yin, J., Fan, Q., Li, Y., Cheng, F., Zhou, P., Xi, P., Sun, S. *J. Am. Chem. Soc.* 2016, 138, 44, 14546–14549.
- 25. Zuo, Y., Bellani, S., Saleh, G., Ferri, M., Shinde, D. V., Zappia, M. I., Buha, J., Brescia, R., Prato, M., Pascazio, R., Annamalai, A., Souza, D. O., Trizio, L. D., Infanate, I., Bonaccorso, F., Manna, L. *J. Am. Chem. Soc.* 2023, 145, 39, 21419–21431.
- 26. Shi, Z., Wang, X., Kang, W. J., Bai, Y. M., Yang, J., Liu, H., Dong, C. K., Yin, P. F. *ACS Applied Energy Materials* 2023, 6, 19, 10012-10019
- 27. Xu, W., Zhang, H., Li, G., Wu, Z. Scientific Reports 2014, 4, 5863.
- 28. Bao, F., Kemppainen, E., Dorbandt, I., Bors, R., Xi, F., Schlatmann, R., Krol, R., Calnan, S. *ChemElectroChem* **2021**, 8, 195 208.
- 29. Wong, D., Li, Q., Han, C., Xing, Z., Yang, X. Appl. Catal. B: Environ 2021, 249, 91 97
- 30. Xu, Y., Yu, X., Ren, T., Liu, S., Wang, Z., Li, X., Wang, L, Wang, H. *ACS Appl. Mater. Interfaces* **2020**, 12, 34728 34735
- 31. Do, H. H., Tekalgne, M. A., Le, Q. V., Cho, J. H., Ahn, S. H., Kim, S. Y. Nano Convergence 2023, 10:6
- 32. Han, H., Park, S., Jang, D., Kim, W. B. J. Alloys Compd. 2021, 853, 157338
- 33. Yan, X., Tian, L., Chen, X. J. Power Sources 2015, 300, 336 343
- 34. Wang, J., Zhan, Z., Shen, C., Liu, H., Pang, X., Gao, M., Mu, J., Cao, M., Li, G. *Catal. Sci. Technol.* **2021**, 11, 2480 2490
- 35. Kuang, Y., Feng, G., Li, P., Bi, Y., Li, Y., Sun, X. Angew, Chem. 2016, 128, 703-707
- 36. Zuo, Y., Bellani, S., Saleh, G., Ferri, M., Shinde, D. V., Zappia, M. I., Buha, J., Brescia, R., Prato, M., Pascazio, R., Annamalai, A., de Souza, D. O., Trizio, L. D., Infante, I., Bonaccorso, F., Manna, L. *J. Am. Chem. Soc.* **2023**, 145, 21419 21431
- 37. Huang, H., Jung, H., Li, S., Kim, S., Han, J. W., Lee, J. Nano Energy 2022, 92, 106763
- 38. Zhai, P., Xia, M., Wu, Y., Zhang, G., Gao, J., Zhang, B., Cao, S., Zhang, Y., Li, Z., Fan, Z., Wang, C., Zhang, X., Miller, J. T., Sun, L., Hou, J. *Nat. Commun.* **2021**, 12, 4587
- 39. Xing, Z., Wang, D., Meng, T., Yang, X. ACS Applied Materials & Interfaces 2020, 12, 39163-39169
- 40. Wang, D., Yang, L., Liu, H., Cao, D. J. Catal. 2019, 375, 249 256
- 41. Yang, X., Zhao, Z., Yu. Xu, Feng, L. Chem. Commun., 2019, 55, 1490 1493
- 42. Zhu, Y., Tahini, H. A., Hu, Z., Dai, J., Chen., Y., Sun, H., Zhou, W., Liu, Meilin Liu, Smith, S. C., Wang, H., Shao, Z. *Nat. Commun.* **2019**, 10, 149 154
- 43. Liu, Y., Liu S., Wang, Y., Zhang, Q., Gu, L., Zhao, S., Xu, D., Li, Y., Bao, J., Dai, Z *J. Am. Chem. Soc.* **2018**, 140, 2731 2734
- Yang, J., Guo, H., Chen, S., Li, Y., Cai, C., Gao, P., Wang, L., Zhang, Y., Sun, R., Niu, X., Wang, Z. J. Mater. Chem. A 2018, 6, 13859 13866
- 45. Wang, Z., Ren, X., Luo, Y., Wang, L., Cui, G., Xie, F., Wang, H., Xie, Y., & Li, T. *Nanoscale* **2018**, 10, 12302-12307